

# Models for infrared emission from *IRAS* galaxies

M. Rowan-Robinson and J. Crawford *Astronomy Unit, Queen Mary College, Mile End Road, London E1 4NS*

Accepted 1988 November 24. Received 1988 November 23; in original form 1986 June 17

**Summary.** The far-infrared (10–100  $\mu\text{m}$ ) spectra of galaxies detected in all four wavelength bands by *IRAS* are modelled in terms of three components: a cool ‘disc’ component; a warmer ‘starburst’ component, and a ‘Seyfert’ component peaking at 25  $\mu\text{m}$ . The luminosity in the ‘disc’ component is well-correlated with the optical luminosity of the galaxy and this component is interpreted as emission from interstellar dust illuminated by the galaxy’s starlight. The ‘starburst’ component is interpreted as being due to a burst of star formation in the galaxy nucleus and its spectrum is fitted well by a model consisting of hot stars embedded in an optically thick dust cloud. The ‘Seyfert’ component is interpreted as being due to a power-law continuum source within a dust cloud presumably associated with the narrow-line region of the compact source. The density distribution in this dust cloud behaves as  $n(r) \propto r^{-1}$ .

The luminosity in the ‘starburst’ component is correlated with Hubble type and whether or not the galaxy has a bar. The luminosity in the ‘Seyfert’ component is correlated with the X-ray luminosity of the galaxy, supporting the hypothesis that the central compact power-law continuum source is responsible for illuminating the dust seen emitting in the far-infrared.

Detailed ultraviolet to submillimetre spectra of several galaxies are compared with the predictions of the models. For the non-Seyfert and many of the Seyferts the proposed models are a good fit, but for NGC 1068 and several other Seyfert galaxies a more complex geometry for the dust distribution is indicated. The observed 1–10  $\mu\text{m}$  spectra can be fitted in several cases with a higher-optical-depth ‘Seyfert’ component, but since a power-law continuum is seen in the ultraviolet for many of these Seyferts, we infer that the dust in the narrow-line region has a non-spherically symmetric geometry, for example being concentrated into clouds. For Arp 220 and NGC 4418, ‘starburst’ models with additional internal or interstellar extinction give a good fit, though a deeply dust-embedded quasar is also a possibility for Arp 220.

## 1 Introduction

Far-infrared (10–100  $\mu\text{m}$ ) radiation can be expected from a normal spiral galaxy due to a variety of mechanisms. Dust in interstellar neutral hydrogen clouds, illuminated by the general

interstellar radiation field, radiates prominently at 100  $\mu\text{m}$  and in our Galaxy has been called the infrared ‘cirrus’ (Low *et al.* 1984). The cirrus is also seen at 60  $\mu\text{m}$  and has been found to be radiating surprisingly strongly at 25 and 12  $\mu\text{m}$  (Gautier & Beichman 1985; Boulanger, Baud & van Albada 1985). To radiate significantly at 12  $\mu\text{m}$ , interstellar grains must include a grain population much hotter than the thermal equilibrium temperature and it has been postulated that this population consists of very small grains (radius 0.001–0.003  $\mu\text{m}$ ,  $\sim 50$  atoms) or, alternatively, of large molecules (Sellgren 1984; Leger & Puget 1984). Dust in the surface layers of molecular clouds will also be heated by the interstellar radiation field and in addition may be heated by young OB associations recently formed from the cloud complex. However, UV photons will not be able to penetrate further than  $A_v \sim 1$  into the clouds, so the bulk of the dust within molecular clouds should be at a temperature significantly lower than that in the H I clouds. Dust in the vicinity of protostars and newly formed stars embedded in molecular clouds will also radiate strongly in the far-infrared. Crawford & Rowan-Robinson (1986) have shown that compact, high-surface-brightness *IRAS* sources in the galactic plane, many of which are associated with compact H II regions, can be modelled as hot stars embedded in a high-optical-depth dust cloud.

Finally, high-optical-depth circumstellar dust shells around late-type stars, OH-IR sources and young planetary nebulae, form a related population of far-infrared emitters which dominate the 12- and 25- $\mu\text{m}$  emission from the bulge of our Galaxy (Habing *et al.* 1985; Rowan-Robinson & Chester 1987) and will contribute to the 10–25  $\mu\text{m}$  emission from the discs of normal spirals.

Turning to active galaxies, some categories like ‘starburst’ galaxies (Balzano 1983) may differ from normal spirals in the far-infrared only in the relative proportions of the different ingredients discussed above. On the other hand, galaxies with a quasar-like nucleus, e.g. Seyfert 1 galaxies, might be expected to produce additional far-infrared radiation. Both quasars and Seyferts are known to have power-law spectra in the wavelength range 1–10  $\mu\text{m}$ , with spectral index  $\alpha$  [ $S(\nu) \propto \nu^{-\alpha}$ ] in the range 0.5–2 (Ward *et al.* 1987; Neugebauer *et al.* 1979). At visible and ultraviolet wavelengths, quasars also have roughly power-law continua with a mean spectral index around 0.5 (Richstone & Schmidt 1980; Cheney & Rowan-Robinson 1981). Where such a nuclear source is located in a galaxy containing dust, for example a spiral galaxy, some of this visible and ultraviolet light will be absorbed by dust and re-emitted in the far-infrared.

In this paper, we show how the far-infrared spectra of a sample of *IRAS* galaxies can be interpreted in terms of these different components. Preliminary results of this work were given by Rowan-Robinson & Crawford (1986) and Rowan-Robinson (1987a,b). Models for infrared emission from normal and starburst *IRAS* galaxies have also been given by Helou (1986) and de Jong & Brink (1987), although these do not involve detailed radiative transfer calculations as in the present work. Rowan-Robinson (1987a,b) has reviewed the differences in the three approaches.

## 2 The sample studied

We have selected from the *IRAS Point Source Catalog* those sources which have high-quality fluxes in all four *IRAS* bands (12, 25, 60, 100  $\mu\text{m}$ ), which are not flagged as associated with months-confirmed small extended sources (SES) in any band, and which are associated with catalogued galaxies. Associations were only accepted if they were within 2 arcmin of the *IRAS* position. Where accurate optical positions are available for the galaxy, the positional agreement with the *IRAS* source is generally better than 10 arcsec for this sample. After deletion of two sources whose far-infrared spectra were clearly those of stars (and for which there were

also stellar associations), of the source 15463–2845 which is flagged as confused, and of the planetary nebula NGC 6543 which picked up a spurious association with a nearby galaxy, the sample consisted of 227 galaxies.

The SES-flag condition was necessary, both to eliminate contamination by cirrus emission and to ensure that the fluxes measured by *IRAS* represent the total flux from the galaxy. Where the emission from a galaxy is extended with respect to the *IRAS* beam, the fluxes reported in the *Point Source Catalog* may be seriously underestimated and corresponding *IRAS* colours will be distorted.

Table 1 summarizes the properties of the 227 galaxies. The columns give: (1) the *IRAS* name; (2) the associated galaxy; (3)–(6) the *IRAS* 12, 25, 60 and 100  $\mu\text{m}$  fluxes; (7) the de Vaucouleurs galaxy type parameter  $T$  (de Vaucouleurs, de Vaucouleurs & Corwin 1976); (8)  $NB = 3$  for galaxies of type S(B), 2 for galaxies of type S(AB) and 1 for galaxies of type S(A), 0 if the bar type is not known (de Vaucouleurs *et al.* 1976); (9)  $B$  or  $m_{pg}$ ; (10) reference for magnitude (1 = Zwicky *et al.* 1968; 2 = Nilson 1973; 3 = de Vaucouleurs *et al.* 1976; 4 = Hewitt & Burbidge 1980; 5 = Lauberts 1982; 6 = Vorontsov-Velyaminov *et al.* 1962–74; 7 = Sandage & Tamman 1981); (11) internal extinction,  $A_{\text{int}}$ , in mag. (de Vaucouleurs *et al.* 1976); (12) interstellar extinction,  $A_{\text{is}}$ , in mag. (Burstein & Heiles 1978); (13) velocity, corrected for galactic rotation; (14) reference for velocity (1 = de Vaucouleurs *et al.* 1976; 2 = Huchra 1988; 3 = de Grijp *et al.* 1985; 4 = Balzano 1983; 5 = Sandage & Tamman 1981; 6 = Roche *et al.* 1986; 7 = Strauss & Davis, personal communication; 8 = Soifer *et al.* 1987; 9 = Lawrence *et al.*, in preparation; 10 = da Costa *et al.* 1985); (15) activity type (1 = Sey 1; 2 = Sey 2; 3 = starburst; 4 = H II galaxy; 5 = faint blue nucleus; 6 = diffuse; 7 = BL Lac or quasar); (16) reference for activity type (1 = Balzano 1983; 2 = Véron-Cetty & Véron 1985; 3 = Weedman 1973; 4 = Huchra 1988; 5 = Lawrence *et al.*, in preparation); (17)–(19) Markarian, Arp or Vorontsov-Velyaminov number. Members of the Fornax, Virgo and Centaurus clusters have been assigned the mean cluster velocities given by Sandage & Tamman (1981).

All but one of the galaxies have measured velocities. Twenty four are elliptical or lenticular; 129 are spiral or irregular; 74 are of unknown Hubble type; 18 are starburst or H II galaxies; 15 are Seyfert 1; 23 are Seyfert 2. Arp, Vorontsov-Velyaminov and Zwicky compact galaxies appear to be represented on a basis proportional to their frequency in the general galaxy population. Because the sample is essentially selected at 12  $\mu\text{m}$ , it is strongly biased towards galaxies with excess emission at 12  $\mu\text{m}$ , i.e. Seyferts (see next section), compared with a sample selected at, say, 60  $\mu\text{m}$ .

### 3 *IRAS* colour–colour diagrams

Fig. 1(a) and (b) show the 12–25–60 and 25–60–100  $\mu\text{m}$  colour–colour diagrams for the sample, with different symbols for starburst (+ H II), Seyfert and other galaxies. Some striking features of this distribution are immediately apparent.

- (i) The starburst galaxies occupy well-defined areas of the two diagrams and in fact have colours very similar to those of compact H II regions in our Galaxy (Crawford & Rowan-Robinson 1986).
- (ii) The bulk of the ‘normal’ galaxies (non-Seyfert, non-starburst) lie in a band stretching from the zone occupied by the starburst galaxies towards warmer S(25)/S(12) colours in Fig. 1(a) and towards cooler S(100)/S(60) colours in Fig. 1(b). Helou (1986) has worked with a similar sample, but with Seyferts removed, and interprets the spread from ‘disc’ to ‘starburst’ colours as being due to an increasing degree of illumination of optically thin interstellar dust.
- (iii) The Seyferts spread out from this band towards lower values of S(60)/S(25), indicating the presence of a component peaking at 25  $\mu\text{m}$ . Such a component was first noticed by Miley

Table 1. Unresolved *IRAS* galaxies with high-quality fluxes in all four bands.

IRAS name	identification	S(12)	S(25)	S(60)	S(100)	T	NB	B	ref.	A <sub>int</sub>	A <sub>is</sub>	V <sub>o</sub>	ref.	NS ref.	Mrk Arp	W
00014+2028	NGC7817	0.49	0.58	5.03	15.04	4	1	11.35	3	0.40	0.12	25558	2	-	-	-
00073+2588	NGC23	0.47	1.15	8.96	15.71	1	3	12.80	3	0.13	0.12	4793	1	3	1	545
00344-3349	ESO350-IG38	0.43	2.52	6.72	4.53	15	0	13.98	1	0.24	0.00	6136	2	4	2	-
00345-2945	NGC174	0.49	1.32	11.38	19.15	1	3	13.70	5	0.24	-	3469	2	-	-	-
00362+5819	MCG+10-02-001	0.57	0.85	8.24	15.38	15	0	15.00	6	0.35	-	2369	9	-	-	-
00506+7248	MCG+12-02-001a	0.95	3.72	21.56	28.23	15	0	18.00	6	0.24	2.00	4953	7	-	-	-
00509+1225	IZw 1	0.54	1.25	2.12	2.42	15	0	13.60	1	0.06	0.16	18276	2	1	2	-
01091-3820	To 1 0109-38	1.09	1.76	1.82	1.94	15	0	13.69	1	0.24	0.00	3241	2	2	2	-
01219+0331	NGC520	0.78	2.85	31.20	47.43	0	0	12.05	3	0.25	0.08	2272	1	-	-	157 231
01384-7615	NGC643B	0.36	0.90	7.50	13.41	15	0	-	-	-	-	3770	2	-	-	-
01403+1323	NGC660	2.02	7.13	65.07	102.41	1	3	11.50	3	0.28	0.12	982	2	-	-	-
01484+2220	NGC695	0.48	0.82	7.95	12.98	-2	0	13.52	1	0.02	0.32	9855	2	-	-	-
02069-2339	MCG-04-06-009	0.40	0.46	3.27	9.42	15	0	-	-	-	-	5281	7	-	-	-
02071+3857	NGC828	0.75	1.03	10.82	25.53	1	0	12.85	1	0.08	0.20	5612	1	-	-	-
02080+3725	NGC834	0.39	0.76	6.38	13.18	20	0	13.04	1	0.30	0.20	4731	2	-	-	-
02140-1134	MCG-02-06-048	0.42	0.74	5.78	11.89	15	0	13.00	6	0.05	0.04	4043	7	-	-	-
02208+4744	UGC1845	0.37	1.24	9.82	15.14	2	0	15.70	1	0.22	1.32	4873	7	-	-	-
02252+3105	NGC931	0.66	1.31	2.71	4.70	3	0	13.71	1	0.43	0.32	5076	2	1	2	1040
02345+2053	NGC992	0.56	1.21	10.00	16.38	20	0	13.33	1	0.09	0.40	4230	2	-	-	-
02360-0653	NGC1022	0.80	3.27	19.77	26.61	1	3	12.20	3	0.06	0.04	1505	1	-	-	-
02398+2821	NGC1056	0.34	0.50	5.40	11.39	1	0	13.33	1	0.14	0.36	830	2	-	-	1183
02401-0013	NGC1068	38.30	86.74	185.44	238.34	3	1	9.51	3	0.06	0.12	1134	1	2	2	37
02435+1253	UGC2238	0.43	0.61	8.23	15.61	10	0	15.20	1	0.21	0.32	6323	8	-	-	-
02509+1248	NGC1134	0.52	0.89	8.91	17.14	20	0	12.83	1	0.36	0.40	3661	2	-	-	200
02568+3637	UGC2456	0.50	2.32	10.26	12.68	-2	3	13.62	1	0.05	0.52	3754	2	2	2	1066
03064-0308	NGC1222	0.50	2.38	12.62	15.31	15	0	14.00	6	0.04	0.16	2692	1	3	1	603
03117+4151	UGC2608	0.47	1.44	8.17	11.51	3	3	13.81	1	0.04	0.72	7190	2	2	2	1073
03164+4119	NGC1275	1.03	3.63	7.09	7.76	-2	0	12.35	3	0.05	0.72	5361	1	7	2	-
03220-3638	NGC1326	0.31	0.79	8.14	13.72	-1	3	11.30	3	0.07	0.00	1486	5	5	3	-
03222-0313	NGC1320	0.34	1.08	2.32	2.74	15	0	14.00	6	0.34	0.12	2978	1	-	-	607
03266+4139	UGC2759	0.56	0.55	4.48	9.40	15	0	14.80	1	0.17	1.08	4375	2	-	-	-
03315+6723	UGC2789	0.39	0.57	5.02	10.97	20	3	17.00	2	0.12	-	3254	2	-	-	-
03317-3618	NGC1365	3.23	11.15	77.84	140.02	3	3	10.14	3	0.20	0.00	1486	5	1	2	-
03344-2103	NGC1377	0.45	1.92	7.12	5.70	-2	0	14.00	6	0.12	0.80	1374	8	-	-	-

Table 1 – continued

03348-3609	NGC1386	0.50	1.44	5.77	9.44	1	0	12.00	7	0.30	0.00	1486	5	2	2	-	
03406+3908	UGC283	0.37	0.53	4.64	8.69	-3	0	13.62	1	0.02	1.08	5077	1	-	-	1405	
03451+6856	UGC2866	1.61	6.19	40.26	49.07	-3	0	15.50	1	0.02	1.44	1431	7	-	-	-	
03514+1546	ZG 351+15	0.35	0.74	5.85	6.84	15	0	15.23	1	0.24	1.04	6701	2	-	-	-	
03524-2038	NGC1482	1.60	4.65	31.20	45.51	0	1	14.00	6	0.09	0.08	1542	1	-	-	-	
04097+0525	UGC2882	0.56	0.81	8.30	15.67	20	0	15.86	1	0.24	0.52	6290	2	-	-	-	
04118-3207	MCG-05-11-006	0.52	2.20	13.46	20.89	-2	0	14.50	6	0.00	0.00	3406	7	-	-	-	
04315-0840	NGC1414	1.39	7.60	33.27	31.70	5	3	13.60	3	0.05	0.20	4643	1	3	1	617	
04326+1904	UGC2094	0.40	0.81	6.18	13.09	20	0	16.50	2	0.38	1.48	7413	2	-	-	-	
04329-1028	A0424-10	0.37	0.80	2.71	3.88	15	0	15.00	6	0.08	0.12	10287	2	1	2	618	
04370-2416	MCG-04-12-003	0.37	0.65	5.85	10.87	3	0	14.00	6	0.38	0.00	4263	8	-	-	-	
05053-0805	NGC1797	0.34	1.33	9.21	12.40	3	0	15.00	6	0.24	0.24	4200	5	3	1	1083	
05054+1118	ZG 0505+17	0.40	1.33	10.26	14.06	15	0	15.40	1	0.24	1.48	5428	2	-	-	-	
05368+4340	UGC0811-002	0.36	0.98	13.85	22.56	15	0	14.00	6	0.00	1.60	5814	7	-	-	-	
05445-1648	NGC2076	0.57	0.52	5.74	20.60	15	0	14.00	6	0.16	0.08	2238	7	-	-	-	
05497-0728	NGC2110	0.39	0.88	4.37	6.05	15	0	14.00	6	0.24	1.44	2155	2	-	-	-	
06140+8220	UGC3435	0.32	0.64	4.34	7.05	15	0	14.60	1	0.33	0.36	4512	7	-	-	-	
06253-4708	PG0355-167	0.34	1.45	9.23	11.68	15	0	14.74	5	0.24	0.24	11620	2	-	-	-	
06456+6054	NGC2273	0.29	0.70	2.20	4.29	20	3	13.71	1	0.04	1.56	6082	2	1	2	-	
06511+4625	UGC374	0.63	1.98	2.74	4.43	7.70	15	0	-	-	0.24	0.00	4440	2	-	-	
06562-6933	NGC2150	0.27	0.59	4.43	3.87	3.34	-2	0	13.62	1	0.02	0.48	4229	1	2	2	3
06907+7103	UGC3426	0.70	2.85	3.87	3.87	3	0	13.62	1	0.02	0.36	4234	1	-	-	-	
07054+1858	UGC34425	0.70	2.85	3.87	3.87	3	0	13.62	1	0.02	0.48	4229	1	2	2	3	
07145-2944	MCG-05-18-002	0.44	1.78	4.34	5.80	1	0	13.80	5	0.21	-	2804	7	-	-	-	
07160-6915	NGC2369	0.77	2.20	19.84	37.11	1	3	12.52	3	0.35	0.12	3017	1	-	-	-	
07202-2908	MCG-05-18-003	0.40	1.24	9.91	17.14	3	3	14.50	6	0.00	0.00	2234	1	-	-	-	
07203+5803	UGC3828	0.31	0.50	3.39	3.39	15	0	14.50	1	0.04	0.24	4611	7	-	-	-	
07256+3355	NGC3388	0.49	1.99	15.89	22.29	15	0	14.56	1	0.18	0.18	3313	2	-	-	-	
07336+3521	NGC2415	0.44	0.95	8.48	13.35	10	0	12.82	3	0.00	0.20	4035	2	-	-	-	
07388+4955	NGC3973	0.31	0.77	1.47	2.07	3	3	13.50	3	0.00	0.20	3779	1	-	-	-	
08014+0615	UGC4203	0.56	2.11	1.82	1.45	15	0	13.98	1	0.12	0.12	6650	1	1	2	79	
09084+0119	NGC2782	0.51	1.10	6.24	9.51	15	0	15.00	6	0.24	1.44	2155	2	2	2	1210	
09437-1107	NGC2665	0.35	0.68	2.32	2.65	15	0	15.00	6	0.24	1.44	2155	2	2	2	620	
09425+7116	MCG-04-21-005	1.10	6.55	0.00	0.00	6	0	15.86	1	0.24	0.00	4440	2	-	-	-	
08171-2501	MCG-04-20-009	0.88	2.74	3.22	2.85	15	0	15.86	1	0.24	0.00	4440	2	-	-	-	
09108+4019	NGC2782	0.51	1.10	6.24	9.51	15	0	15.00	6	0.24	1.44	2155	2	2	2	620	

Table 1 - continued

Table 1 - continued

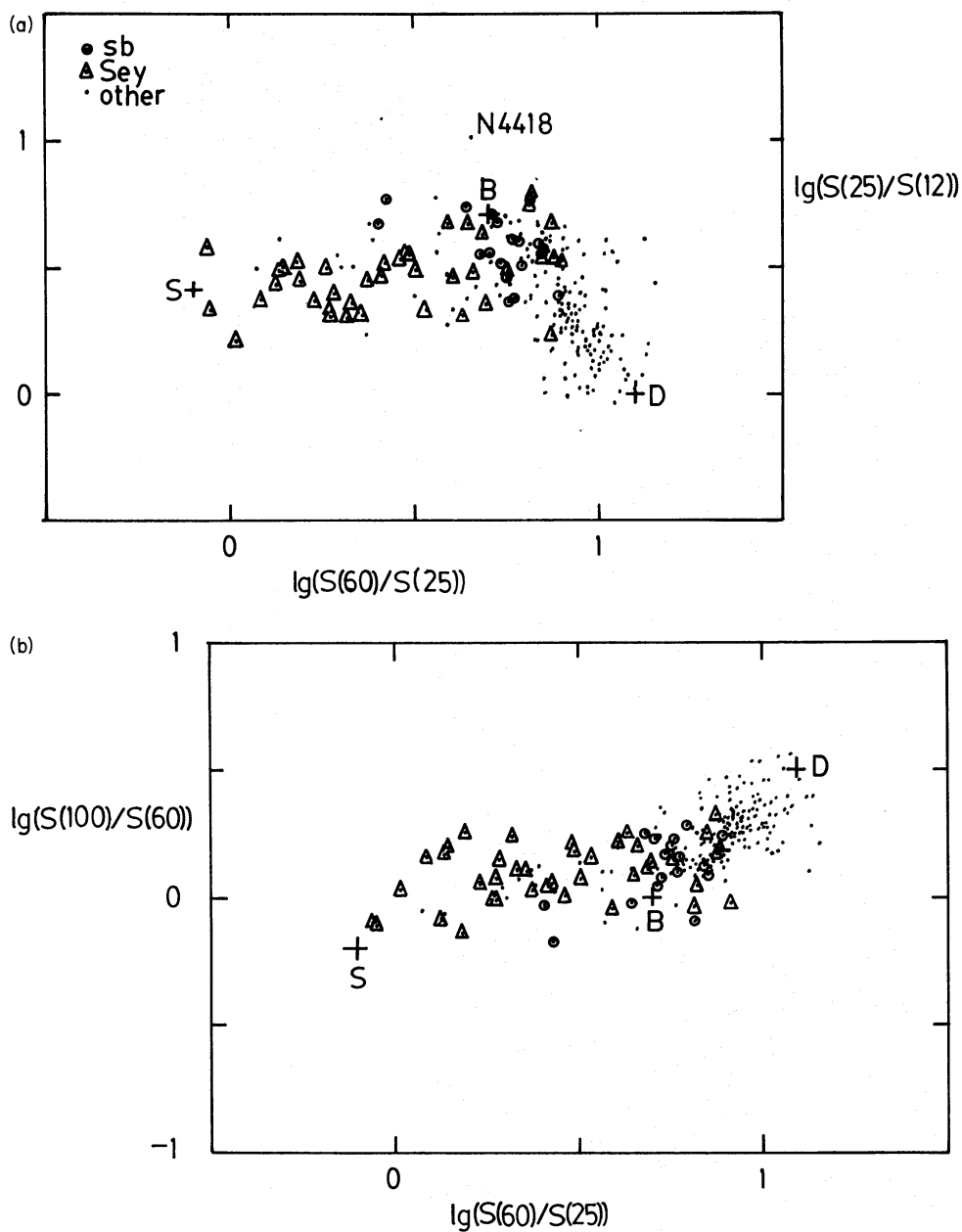
11449+5614	NGC3888	0.37	0.48	4.80	11.05	5	2	13.09	3	0.08	0.00	2541	1	188	-	
11506-3851	ESO320-G30	0.57	2.31	33.90	43.53	15	0	-	-	0.05	0.00	2817	7	-	-	
12002+4854	NGC4047	0.37	0.39	3.64	10.14	3	1	13.10	3	0.17	0.00	3493	2	-	-	
12038+5259	NGC4102	1.46	6.88	47.03	67.35	3	2	12.30	3	0.17	0.00	986	1	-	-	
12116+5448	NGC4194	0.86	4.38	22.46	25.15	10	3	12.95	3	0.17	0.00	2629	1	3	1	
12131+3636	NGC4214	0.39	1.77	14.36	24.95	10	2	10.20	3	0.10	0.00	309	1	-	-	
12159+3005	NGC4253	0.41	1.39	4.02	4.07	1	3	13.52	1	0.03	0.04	3869	2	1	2	
12173+0537	NGC4273	0.60	1.19	9.82	21.29	5	3	12.31	3	0.14	0.00	2188	1	-	-	
12232+1256	NGC4388	1.00	3.56	10.69	17.22	3	1	11.83	3	0.45	0.04	1026	5	2	2	
12243-0036	NGC4418	0.94	9.62	43.46	32.97	15	0	13.69	1	0.24	0.00	2055	6	-	-	
12244+1519	NGC4419	0.55	1.47	7.73	17.43	1	3	11.95	3	0.34	0.04	1026	5	-	-	
12250-0800	NGC4433	0.60	1.45	13.28	15.42	2	2	13.01	3	0.26	0.08	2746	1	-	-	
12265+0216	NGC4273	0.54	0.93	2.16	2.78	15	0	13.07	4	0.24	0.00	47300	3	7	2	
12290+5814	NGC4500	0.30	0.69	3.95	6.67	1	3	13.04	1	0.13	0.00	3128	1	3	1	
12329-3938	NGC4507	0.46	1.41	4.50	5.37	-1	2	12.64	3	0.04	0.32	3283	2	2	2	
12381-3628	T01_1238-364	0.66	2.33	7.09	10.78	15	0	14.40	5	0.24	0.24	3060	2	2	-	
12412+1639	NGC4651	0.39	0.41	5.08	14.86	5	1	11.30	3	0.12	0.00	1026	5	-	189	
12456-0303	NGC4691	0.72	2.45	15.01	21.15	0	3	11.70	3	0.06	0.00	987	1	-	-	
12483+7308	NGC4750	0.38	0.39	4.41	14.05	2	1	12.26	3	0.03	0.08	1698	1	-	-	
12493+7154	NGC4749	0.32	0.40	4.63	11.49	3	0	14.00	1	0.49	0.08	1916	2	-	-	
12517-1015	NGC4781	0.55	0.65	7.79	17.63	7	3	11.69	3	0.24	0.04	744	1	-	-	
12522+2912	NGC4793	0.66	1.18	11.47	27.32	5	2	12.30	3	0.19	0.04	2481	1	-	-	
12523+4648	NGC4800	0.36	0.48	4.98	14.33	3	1	12.30	3	0.09	0.00	831	1	-	-	
12532+0434	NGC4808	0.68	0.70	6.71	14.74	6	1	12.56	3	0.26	0.00	679	1	-	-	
12540+5708	NGC4858	1.82	8.53	33.19	30.00	5	1	14.30	3	0.14	0.00	12556	1	2	231	
12540-0717	IC3398	0.50	0.77	8.13	15.45	15	0	14.00	6	0.41	0.04	912	8	-	-	
12542-0815	NGC4818	0.85	3.88	19.88	25.73	2	2	11.89	3	0.33	0.04	1012	2	-	-	
12554+0150	NGC4845	0.44	0.69	9.36	23.20	2	1	12.17	3	0.40	0.00	1128	2	-	-	
12580+0246	NGC4900	0.34	0.47	5.35	11.76	5	3	12.10	3	0.02	0.00	945	1	-	-	
13035-4008	ESO323-G77	0.68	1.25	5.43	8.65	15	0	-	-	-	-	4251	2	1	4	
13062-1514	NGC4984	0.71	1.71	11.20	15.18	-1	2	11.71	7	0.06	0.08	1101	2	-	-	
13098-1716	MCG-03-34-014	0.56	0.71	6.73	15.82	15	0	12.50	6	0.45	0.12	2586	7	-	-	
13136+6223	UGC8335	0.41	1.93	11.14	10.39	15	0	14.22	1	0.30	0.00	9606	2	-	238	
13142-1622	MCG504	0.62	1.05	11.31	27.63	4	1	11.51	7	0.17	0.16	1587	2	-	-	
13170-2708	MCG-03-34-063	0.65	0.74	8.75	31.98	1	1	12.50	9	0.22	0.24	2011	10	-	-	
13197-1627	MCG-03-34-065	0.68	2.51	16.05	5.62	15	0	14.50	6	0.42	0.16	4858	3	-	2	
13229-2934	NGC5135	0.68	2.52	30.23	3	12.94	2	3	12.94	3	0.30	0.00	3923	2	2	2
13286-3432	NGC5188	0.76	2.82	6.24	11.78	20	0	13.42	1	0.08	0.00	1313	2	-	0.24	
13291		3	12.70	3	34.66	3	3	12.70	3	0.24	0.24	2129	1	-	-	

Table 1 – continued

13301-2857	IC4280	0.41	0.72	5.82	11.82	3	0	13.50	6	0.05	0.24	4749	7	
13304+6301	NGC5218	0.35	0.93	7.21	14.16	3	3	13.10	3	0.18	0.00	3027	2	
13370-3123	NGC5253	2.59	12.20	30.85	28.99	0	0	10.99	3	0.25	0.24	255	5	
13373+0105	NGC5258	0.57	1.31	10.16	17.86	3	1	13.40	1	0.11	0.00	6615	1	
13464-3003	IC4329A	1.06	2.26	2.00	1.55	0	1	14.15	3	0.34	0.24	4640	1	
13477-4848	ESO211-IG10	0.67	1.68	12.91	72.50	15	0	12.60	5	0.24	0.84	3184	2	
13510+3244	NGC5347	0.34	0.94	1.45	2.62	2	3	13.40	3	0.06	0.00	2403	2	
13526+1836	UGC8850	0.60	1.61	2.15	1.78	15	0	14.67	1	0.28	0.00	15149	2	
13550+4205	NGC5383	0.36	0.65	5.23	12.60	3	3	12.05	3	0.05	0.00	2354	1	
13591+5324	NGC5430	0.52	1.65	10.23	19.82	3	3	12.78	3	0.15	0.00	2981	2	
14045+5527	NGC5480	0.27	0.43	3.63	9.71	5	1	12.89	3	0.13	0.00	1928	1	
14092-6306	CIRCINUS	18.86	68.48	248.62	313.72	3	1	11.25	3	0.33	2.00	214	6	
14106-0238	NGC5506	1.30	3.68	8.65	9.37	1	0	13.21	1	0.36	0.12	1690	1	
14152-4309	NGC5530	0.33	0.39	3.76	12.87	4	1	11.98	3	0.21	0.36	1012	2	
14179-4604	ESO272-G5	0.52	1.15	9.40	16.83	15	0	-	-	1527	7	-	-	
14188+7148	NGC5607	0.31	0.74	4.35	6.31	15	0	13.71	1	0.03	0.08	7941	1	
14214+4511	NGC5600	0.40	0.61	5.52	11.20	5	0	13.20	3	0.01	0.00	2365	2	
14280+3126	NGC5653	0.76	1.37	10.81	20.50	3	1	12.90	3	0.06	0.00	3642	1	
14288+3532	NGC5656	0.28	0.30	2.69	7.61	2	1	12.56	1	0.08	0.00	3092	1	
14299+0817	NGC5655	0.41	0.79	6.53	12.73	5	2	12.79	3	0.12	0.08	2264	1	
14349+5900	UGC9412	0.40	1.24	2.27	2.22	15	0	14.11	3	0.22	0.00	3606	2	
14351+0230	NGC5590	0.41	0.48	6.35	15.66	5	0	12.50	3	0.38	0.00	1729	2	
14383-0006	NGC5719	0.58	0.81	8.17	16.73	2	2	13.40	1	0.32	0.00	1680	2	
14454-4343	ESO273-IG04	0.55	1.80	4.74	5.35	15	0	14.70	5	0.24	0.52	11360	2	
14483+0519	NGC5765	0.29	0.83	3.34	5.42	15	0	14.31	1	0.07	0.12	8342	2	
14544-4255	IC4518	0.38	1.33	2.62	13.60	15	0	-	-	2897	7	-	-	
14556-4148	ESO327-G37	0.34	0.67	4.97	14.61	15	0	-	-	4966	2	-	-	
15005+3243	TGCP668	0.32	0.91	5.10	17.48	15	0	13.62	1	0.22	0.20	4138	2	
15187-1254	NGC5955	0.43	1.36	10.60	15.50	2	3	12.89	3	0.10	0.52	2230	1	
15243+4150	NGC5929	0.40	1.65	9.40	13.40	2	0	12.85	1	0.02	0.00	2696	1	
15276+1309	NGC5936	0.48	1.28	8.71	16.00	3	3	13.00	3	0.02	0.08	4078	2	
15437-0234	NGC5990	0.63	1.70	9.74	15.32	1	0	12.74	1	0.20	0.24	3848	2	
15456-1339	NGC5995	0.44	0.90	3.81	6.80	15	0	14.50	6	0.05	0.56	2297	7	
16104+2325	NGC6000	1.23	3.62	9.80	20	9.49	15	0	13.00	6	0.05	0.20	2029	2
16180-3753	NGC6120	0.36	1.18	3.36	6.36	15	0	13.81	1	0.27	0.00	6146	2	
16301+1955	NGC6181	0.51	1.05	3.93	7.80	15	0	14.11	1	0.00	0.00	9400	1	
16504+0228	NGC6240	0.28	0.52	1.41	3.62	15	0	12.50	3	0.24	0.24	2512	1	
16511	-	23.11	8.78	3.93	7.80	15	0	14.48	1	0.22	0.00	817	-	
16512	-	25.76	11	9.93	19.93	5	2	12.50	3	0.24	0.24	496	1	
16513	-	25.76	11	9.93	19.93	5	0	14.48	1	0.22	0.00	817	-	
16514	-	25.76	11	9.93	19.93	5	2	12.50	3	0.24	0.24	496	1	
16515	-	25.76	11	9.93	19.93	5	0	14.48	1	0.22	0.00	817	-	
16516	-	25.76	11	9.93	19.93	5	2	12.50	3	0.24	0.24	496	1	
16517	-	25.76	11	9.93	19.93	5	0	14.48	1	0.22	0.00	817	-	
16518	-	25.76	11	9.93	19.93	5	2	12.50	3	0.24	0.24	496	1	
16519	-	25.76	11	9.93	19.93	5	0	14.48	1	0.22	0.00	817	-	
16520	-	25.76	11	9.93	19.93	5	2	12.50	3	0.24	0.24	496	1	
16521	-	25.76	11	9.93	19.93	5	0	14.48	1	0.22	0.00	817	-	
16522	-	25.76	11	9.93	19.93	5	2	12.50	3	0.24	0.24	496	1	
16523	-	25.76	11	9.93	19.93	5	0	14.48	1	0.22	0.00	817	-	
16524	-	25.76	11	9.93	19.93	5	2	12.50	3	0.24	0.24	496	1	
16525	-	25.76	11	9.93	19.93	5	0	14.48	1	0.22	0.00	817	-	
16526	-	25.76	11	9.93	19.93	5	2	12.50	3	0.24	0.24	496	1	
16527	-	25.76	11	9.93	19.93	5	0	14.48	1	0.22	0.00	817	-	
16528	-	25.76	11	9.93	19.93	5	2	12.50	3	0.24	0.24	496	1	
16529	-	25.76	11	9.93	19.93	5	0	14.48	1	0.22	0.00	817	-	
16530	-	25.76	11	9.93	19.93	5	2	12.50	3	0.24	0.24	496	1	
16531	-	25.76	11	9.93	19.93	5	0	14.48	1	0.22	0.00	817	-	
16532	-	25.76	11	9.93	19.93	5	2	12.50	3	0.24	0.24	496	1	
16533	-	25.76	11	9.93	19.93	5	0	14.48	1	0.22	0.00	817	-	
16534	-	25.76	11	9.93	19.93	5	2	12.50	3	0.24	0.24	496	1	
16535	-	25.76	11	9.93	19.93	5	0	14.48	1	0.22	0.00	817	-	
16536	-	25.76	11	9.93	19.93	5	2	12.50	3	0.24	0.24	496	1	
16537	-	25.76	11	9.93	19.93	5	0	14.48	1	0.22	0.00	817	-	
16538	-	25.76	11	9.93	19.93	5	2	12.50	3	0.24	0.24	496	1	
16539	-	25.76	11	9.93	19.93	5	0	14.48	1	0.22	0.00	817	-	
16540	-	25.76	11	9.93	19.93	5	2	12.50	3	0.24	0.24	496	1	
16541	-	25.76	11	9.93	19.93	5	0	14.48	1	0.22	0.00	817	-	
16542	-	25.76	11	9.93	19.93	5	2	12.50	3	0.24	0.24	496	1	
16543	-	25.76	11	9.93	19.93	5	0	14.48	1	0.22	0.00	817	-	
16544	-	25.76	11	9.93	19.93	5	2	12.50	3	0.24	0.24	496	1	
16545	-	25.76	11	9.93	19.93	5	0	14.48	1	0.22	0.00	817	-	
16546	-	25.76	11	9.93	19.93	5	2	12.50	3	0.24	0.24	496	1	
16547	-	25.76	11	9.93	19.93	5	0	14.48	1	0.22	0.00	817	-	
16548	-	25.76	11	9.93	19.93	5	2	12.50	3	0.24	0.24	496	1	
16549	-	25.76	11	9.93	19.93	5	0	14.48	1	0.22	0.00	817	-	
16550	-	25.76	11	9.93	19.93	5	2	12.50	3	0.24	0.24	496	1	
16551	-	25.76	11	9.93	19.93	5	0	14.48	1	0.22	0.00	817	-	
16552	-	25.76	11	9.93	19.93	5	2	12.50	3	0.24	0.24	496	1	
16553	-	25.76	11	9.93	19.93	5	0	14.48	1	0.22	0.00	817	-	
16554	-	25.76	11	9.93	19.93	5	2	12.50	3	0.24	0.24	496	1	
16555	-	25.76	11	9.93	19.93	5	0	14.48	1	0.22	0.00	817	-	
16556	-	25.76	11	9.93	19.93	5	2	12.50	3	0.24	0.24	496	1	
16557	-	25.76	11	9.93	19.93	5	0	14.48	1	0.22	0.00	817	-	
16558	-	25.76	11	9.93	19.93	5	2	12.50	3	0.24	0.24	496	1	
16559	-	25.76	11	9.93	19.93	5	0	14.48	1	0.22	0.00	817	-	
16560	-	25.76	11	9.93	19.93	5	2	12.50	3	0.24	0.24	496	1	
16561	-	25.76	11	9.93	19.93	5	0	14.48	1	0.22	0.00	817	-	
16562	-	25.76	11	9.93	19.93	5	2	12.50	3	0.24	0.24	496	1	
16563	-	25.76	11	9.93	19.93	5	0	14.48	1	0.22	0.00	817	-	
16564	-	25.76	11	9.93	19.93	5	2	12.50	3	0.24	0.24	496	1	
16565	-	25.76	11	9.93	19.93	5	0	14.48	1	0.22	0.00	817	-	
16566	-	25.76	11	9.93	19.93	5	2	12.50	3	0.24	0.24	496	1	
16567	-	25.76	11	9.93	19.93	5	0	14.48	1	0.22	0.00	817	-	
16568	-	25.76	11	9.93	19.93	5	2	12.50	3	0.24	0.24	496	1	
16569	-	25.76	11	9.93	19.93	5	0	14.48	1	0.22	0.00	817	-	
16570	-	25.76	11	9.93	19.93	5	2	12.50	3	0.24	0.24</			

Table 1 - continued

17366+8646	UGC10923	0.32	0.55	4.63	9.84	15	0	14.11	1	0.09	0.28	7739	2
17530+3446	UGC11041	0.37	0.72	5.89	13.13	2	0	13.71	1	0.17	0.32	5035	2
18001+6638	NGC6552	0.23	1.08	2.58	2.87	15	0	14.45	1	0.12	0.16	3105	2
18907-6006	ESO140-G12	0.40	1.04	5.62	9.18	15	0	-	-	-	-	3034	7
18095+1458	NGC6574	0.93	1.69	14.27	27.19	4	2	12.85	3	0.08	0.84	2509	1
18329+5950	UGC11284	0.41	1.07	8.67	14.68	15	0	15.30	1	0.32	0.20	9300	9
18341-5732	ESO140-G33	0.38	1.33	14.19	25.57	15	0	-	-	-	-	4496	7
18401-6225	F 51	0.43	0.88	2.00	2.54	15	0	14.80	5	0.24	0.32	4085	2
19070+5051	NGC6764	0.38	1.35	6.44	11.53	3	3	13.04	1	0.18	0.24	2661	2
19385-7045	NGC6808	0.64	0.84	6.79	17.47	1	1	13.39	7	0.30	0.28	3318	2
19393-5846	NGC6810	1.06	3.51	17.84	33.67	2	0	12.21	7	0.42	0.16	1713	1
19414+4510	UGC1466	0.40	0.86	9.00	16.11	15	0	13.50	1	0.18	0.96	1048	9
19517-1241	NGC6835	0.53	1.59	11.44	16.88	1	3	13.40	3	0.45	0.60	1715	1
19582-3833	ESO339-G25	0.50	0.49	3.32	6.57	15	0	-	-	-	-	5035	7
20243-0226	ZZW 83	0.39	0.92	1.11	1.60	15	0	15.20	1	0.24	0.40	8995	9
20264+2533	NGC6921	0.58	1.06	10.93	17.08	0	1	15.00	2	0.39	1.48	4590	1
20272-4738	NGC6918	0.33	1.36	9.28	13.06	1	0	-	-	-	-	1848	2
20414-1054	Mkn 509	0.35	0.74	1.38	1.35	15	0	13.00	5	0.24	0.20	10521	2
20481-5715	IC5063	1.17	3.87	5.89	4.26	-3	1	13.05	3	0.02	0.24	3405	1
20551-4250	ESO286-IG19	0.33	1.91	12.43	10.15	15	0	14.40	5	0.24	0.08	12783	2
21193-3953	ESO402-G26	0.32	0.78	6.79	10.82	15	0	-	-	-	-	2833	2
21453-3511	IC5135	0.63	2.15	16.34	25.43	15	0	13.00	3	0.03	0.00	4875	1
21591-3206	NGC7172	0.46	0.78	5.83	12.38	2	0	12.82	3	0.18	0.00	2698	1
22132-3705	IC5179	1.13	2.18	19.15	36.06	4	1	12.50	3	0.22	0.00	3466	2
23007+0836	NGC7469	1.30	5.49	26.60	34.35	1	2	12.60	3	0.10	0.12	5102	1
23121+0415	NGC7541	0.92	1.56	18.19	38.89	4	3	12.45	3	0.32	0.16	2860	1
23128-5919	ESO148-IG02	0.30	1.66	10.74	9.91	15	0	14.70	5	0.24	0.00	13163	2
23134-4251	NGC7552	2.99	12.01	72.56	99.47	2	3	11.40	3	0.10	0.12	1636	1
23135+2516	MCG+04-54-038	0.34	1.70	9.54	11.95	15	0	15.00	1	0.00	0.24	8466	8
23260-4136	IC5325	1.36	6.38	47.70	71.54	2	3	11.40	3	0.26	0.00	1427	1
23156-4238	NGC7582	1.36	6.38	4.36	14.90	4	0	12.31	3	0.00	0.00	1440	2
23179+1657	NGC7625	0.58	1.03	8.92	18.17	1	1	12.80	3	0.02	0.12	1864	1
23179+2702	NGC7624	0.32	0.32	3.00	8.42	5	0	14.10	3	0.10	0.24	4729	1
23259+2208	NGC7678	0.42	0.89	7.10	14.60	5	2	12.80	3	0.10	0.12	3695	1
23262+0314	NGC7679	0.51	1.17	7.35	9.63	-2	3	13.25	3	0.07	0.12	5333	1
23488+2018	A2348+2018	0.53	2.46	16.84	20.48	1	0	14.67	1	0.12	0.12	331	-
23488+1949	NGC7771	0.68	1.73	17.93	37.89	1	3	13.10	3	0.26	0.12	4510	1
										0.12	0.12	3871	1
										0.12	0.12	331	-



**Figure 1.** IRAS colour-colour diagrams for unresolved IRAS galaxies with high-quality fluxes in all four bands. Circled dots are starburst (or H II) galaxies, triangles are Seyferts, dots are neither of these or unclassified to date. The crosses labelled D, B, S, are the adopted colours of the ‘disc’, ‘starburst’ and ‘Seyfert’ components used to synthesize the observed far-infrared spectra.

(a)  $\log[S(25)/S(12)]$  versus  $\log[S(60)/S(25)]$ , (b)  $\log[S(100)/S(60)]$  versus  $\log[S(60)/S(25)]$ .

*et al.* (1984) in 3C390.3. Low values of  $S(60)/S(25)$  have been successfully used as a criterion for selecting Seyfert galaxies by Carter (1984), de Grijp *et al.* (1985) and Osterbrock & de Robertis (1985).

#### 4 A three-component model for far-infrared spectra of galaxies

As a first step towards understanding the range of galaxy far-infrared spectra implied by Fig. 1, we postulate that these spectra can be considered as a mixture of three components: (1) a normal ‘disc’ component, (2) a ‘starburst’ component and (3) a ‘Seyfert’ component. The

colours adopted for these components are indicated in Fig. 1 by the letters D, B and S, and Fig. 2 shows the corresponding spectra, normalized to 12  $\mu\text{m}$ , after colour-correction for the effect of the *IRAS* pass-bands. In order to keep the number of parameters to a minimum, our components are assumed to be mutually independent. We shall see that this is entirely consistent with our models for the components, and, as Fig. 2 shows, the component spectra are sufficiently dissimilar that slight changes in their shape should not affect our results. We re-emphasize that the components of Fig. 2 are empirical spectra, representing extremes in the colour distributions of *IRAS* galaxies. We now discuss models for each of these components.

In Fig. 3(a) the spectrum of the 'disc' component is compared with the spectrum of an isolated piece of cirrus in our Galaxy, a small cloud of interstellar neutral gas and dust with  $A_v \sim 0.15$ , presumably illuminated by the interstellar radiation field (Boulanger *et al.* 1985). As the spectrum of the interstellar dust emission has been found to be very uniform over the sky (Burton *et al.* 1986), this cloud can be taken as representative of the interstellar dust in our Galaxy. The agreement is remarkably good, showing that it is plausible to regard the 'disc' component as radiation from interstellar dust in the galaxy illuminated by the general starlight. A theoretical spectrum of the cirrus calculated by Draine & Anderson (1985) for a grain mixture including very small grains is also shown. The agreement with the 'disc' component's spectrum is poor at 12 and 60  $\mu\text{m}$ . If the Draine & Anderson spectrum proved to be a correct estimate of the spectrum of interstellar dust, then the 'disc' component would have to be due to a mixture of emission from cirrus, from warmer dust in the vicinity of newly-forming stars and, perhaps, (at 12  $\mu\text{m}$ ) emission from late-type stars with circumstellar dust shells spread through the galactic disc. Rowan-Robinson & Chester (1987) have estimated that emission from the bulge component identified by Habing *et al.* (1985) would not make a significant contribution to the integrated flux from most galaxies at 12–100  $\mu\text{m}$ . Because the infrared spectrum of very

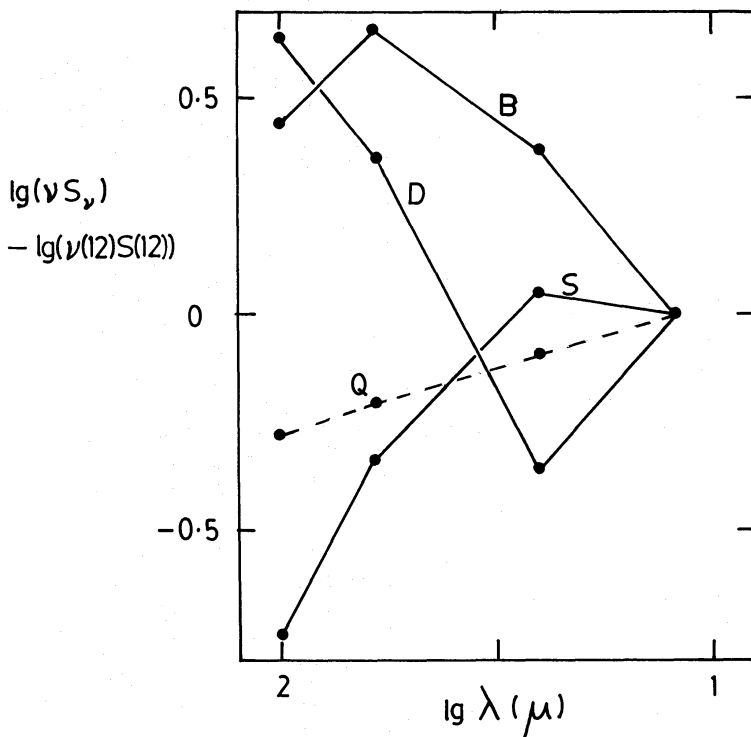


**Figure 2.** 12–100  $\mu\text{m}$  spectra, normalized to 12  $\mu\text{m}$ , of adopted model components: D ('disc'), B ('starburst') and S ('Seyfert'). The broken curve Q is the  $\alpha = 0.7$  power-law ('quasar') component considered in Section 5. The spectra have been colour-corrected, as described in the Appendix.

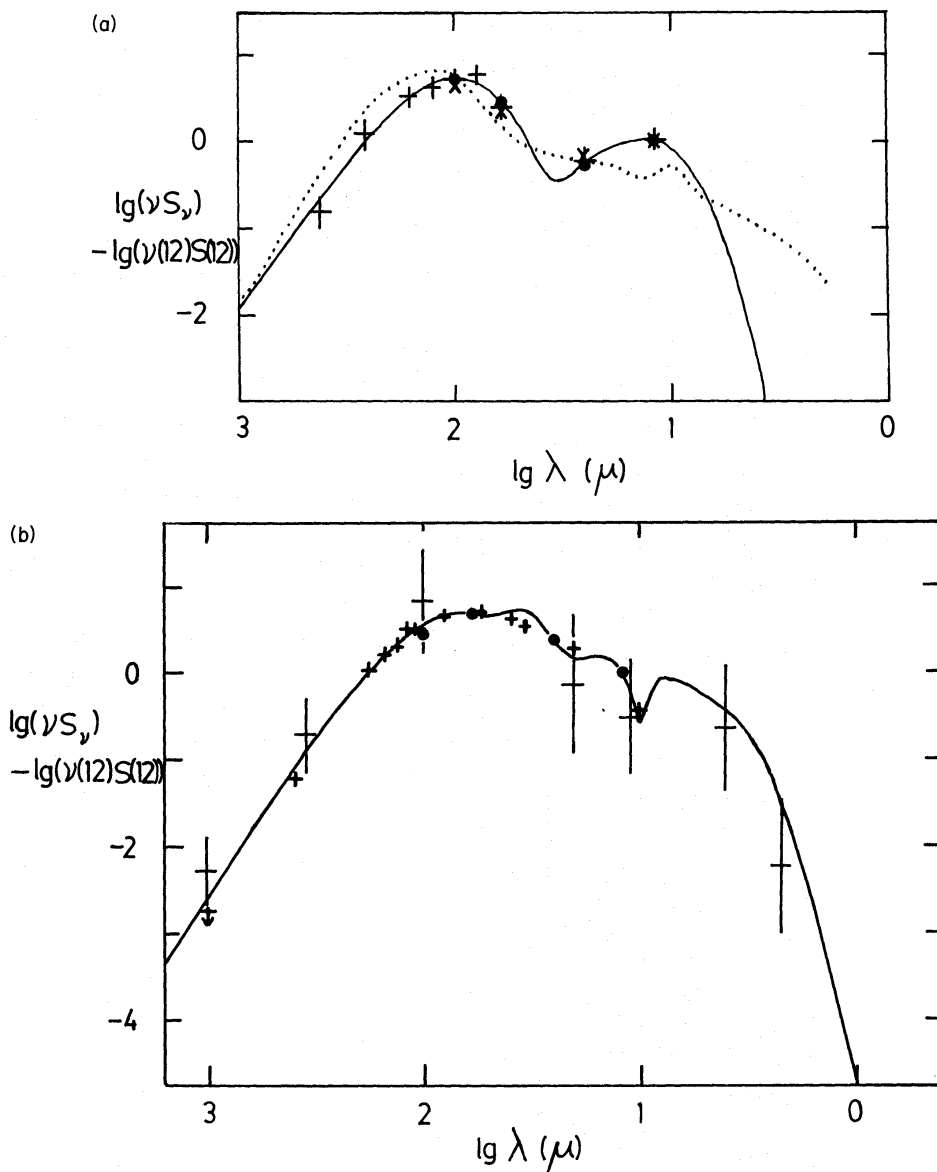
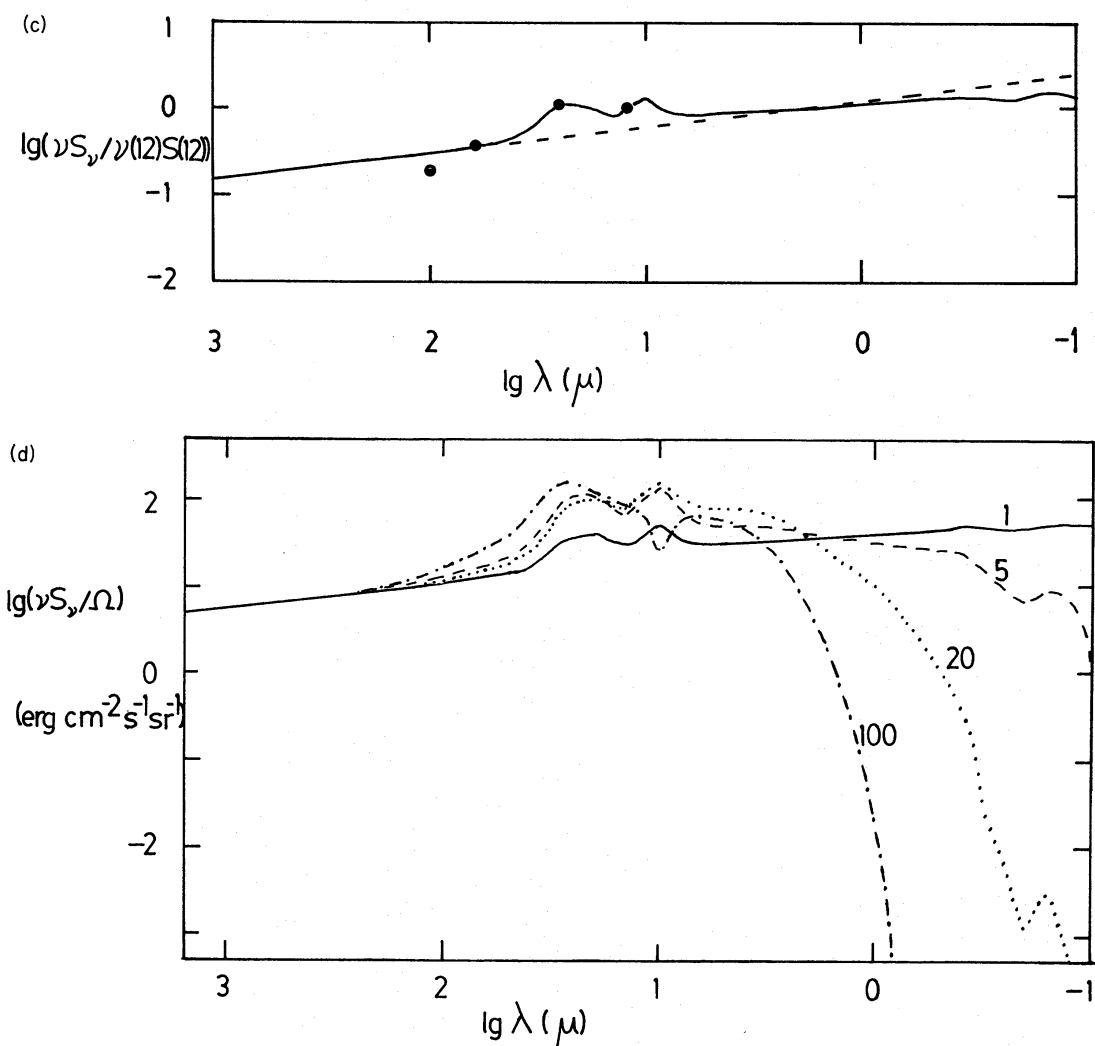


Figure 3. Model fits to the spectra of the adopted components (filled circles).

(a) 'Disc' component. The x's denote the spectrum of an isolated cirrus cloud in our Galaxy studied by Boulanger, Baud & van Albada (1985). The crosses denote a composite spectrum of our Galaxy, compiled from Hauser *et al.* (1984), Caux & Serra (1986) and Pajot *et al.* (1986), by Cox & Mezger (1988). The dotted curve is the interstellar grain model of Draine & Anderson (1985). The solid curve is an empirical fit of the form  $S_\nu = \alpha \nu B_\nu(30 \text{ K}) + \beta \nu B_\nu(210 \text{ K})$ , with  $\alpha$  and  $\beta$  denoting the normalizing constants.

(b) 'Starburst' component. The small crosses are the data of Telesco *et al.* (1984) for the 3-kpc ring in NGC 1068, which they attribute to a starburst. The large crosses are the average spectrum for regions of massive star formation in our Galaxy, derived by Rowan-Robinson (1979). The solid curve is a simple model for a star-forming region of the type discussed by Crawford & Rowan-Robinson (1986), a uniform spherically symmetric dust cloud illuminated by a hot star ( $T_s = 40\,000 \text{ K}$ ), with optical depth  $\tau_{uv} = 100$ , and ratio of inner to outer cloud radius  $r_1/r_2 = 0.0015$ .

small grains remains controversial, we have merely fitted our 'disc' component with a spectrum of the form  $\alpha \nu B_\nu(30 \text{ K}) + \beta \nu B_\nu(210 \text{ K})$  (where  $\alpha$  and  $\beta$  are normalizing constants). The cool component gives a good representation of the 30–100  $\mu\text{m}$  contribution of the larger (0.01–0.1  $\mu\text{m}$ ) grains modelled by Rowan-Robinson (1986), but the hot component will give only a very



**Figure 3 – continued**

(c) ‘Seyfert’ component. The solid curve is a model consisting of an  $\alpha = 0.7$  power-law continuum source (indicated by the broken line) embedded in a spherically symmetric dust cloud with density distribution  $n(r) \propto r^{-1}$ ,  $r_1 \leq r \leq r_2$ , optical depth  $\tau_{uv} = 1$  ( $A_v = 0.23$ ), temperature of the hottest grains  $T_1 = 1000$  K, and  $r_1/r_2 = 0.0055$ .

(d) A sequence of models of the type shown in Fig. 3(c), with  $\tau_{uv} = 1, 5, 20$  and 100.

approximate representation of the very small grains postulated by Sellgren (1984), Leger & Puget (1984), Boulanger *et al.* (1985) and Draine & Anderson (1985). Nevertheless, we shall show in Section 6 that our approximation to the hot component is unlikely to underestimate seriously the 12 to 25  $\mu\text{m}$  flux from the ‘disc’ component.

Fig. 3(b) shows the spectrum of the ‘starburst’ component compared with the spectrum of the 3-kpc disc observed in NGC 1068 by Telesco, Becklin & Wynn-Williams (1984), and with a simple model for a cloud containing a newly formed massive star (stellar temperature  $T_s = 40\,000$  K, grain condensation temperature  $T_1 = 1000$  K, uniform density, ratio of inner radius of dust cloud,  $r_1$ , to outer radius,  $r_2$ ,  $r_1/r_2 = 0.0015$ , composite interstellar grain properties adopted by Rowan-Robinson (1982), ultraviolet optical depth  $\tau_{uv} = 100$ ). The latter model is one from a sequence used by Crawford & Rowan-Robinson (1986) for high-surface-brightness sources in the galactic plane associated with star-forming regions and compact H II regions. The models presented in Fig. 3(b)–(d) were calculated using the radiative transfer

codes of Rowan-Robinson (1980). The agreement of the 'starburst' component spectrum with the model, and with the spectrum of the 3-kpc disc in NGC 1068 which Telesco *et al.* (1984) argue to be a burst of star formation, is excellent. The average spectrum of star-forming clouds in our Galaxy (Rowan-Robinson 1979) is also shown.

For the 'Seyfert' component it is natural to explore models in which dust surrounding the central power-law continuum source absorbs visible and ultraviolet light from the central source and re-emits in the infrared. A problem here is the considerable range of ultraviolet to infrared continua of 'Seyferts' (see Fig. 9 below), showing that a single model cannot fit all sources. Moreover, it is known that the gas in the narrow-line region of 'Seyferts' is clumped into clouds, so it is unlikely that the geometry of the dust distribution can be simple. On the other hand, the far-infrared (12–100  $\mu\text{m}$ ) spectra of Seyferts, after allowance for the possible presence of a 'starburst' component, are remarkably homogeneous, tending to show the characteristic peak at 25  $\mu\text{m}$  seen in Fig. 2 (component S). We therefore explore models for such a spectrum, bearing in mind that such models are likely to be over-simplified.

The input spectrum was assumed to be a power law extending from  $\lambda = 0.1 \mu\text{m}$  to 1 mm. Spectral indices in the range 0.5–1.5 were considered: results are shown here for  $\alpha = 0.7$ , the value about which the 12–100  $\mu\text{m}$  spectral indices of quasars detected by *IRAS* centre (Neugebauer, Soifer & Rowan-Robinson 1986). It also represents a compromise between the value of 0.5 found for the optical–ultraviolet spectra of quasars (Richstone & Schmidt 1980; Cheney & Rowan-Robinson 1981) and the value of 1.0 found for the overall X-ray to far-infrared spectra of Seyfert I continua by Carleton *et al.* (1987) and Edelson, Malkan & Rieke (1987). The 12–100  $\mu\text{m}$  spectrum of the models is found to be insensitive to the value of  $\alpha$  for  $0.5 \leq \alpha \leq 1.0$ .

The dust was assumed to have a spherically symmetric distribution, with a power-law density distribution,  $n(r) \propto r^{-\beta}$ ,  $r_1 \leq r \leq r_2$ . The inner edge of the cloud at  $r_1$  was defined by the condition that the dust temperature be 1000 K. Models with a range of optical depths and  $\beta = 0, 1, 2$  were explored. It was found that the parameter  $\beta$  is critical in defining an emission peak at 25  $\mu\text{m}$ : only for  $\beta = 1$  could this be achieved. The outer radius of the cloud,  $r_2$ , was not a very critical parameter. Fig. 3(d) shows a series of models with  $\beta = 1$  and the ultraviolet optical depth,  $\tau_{\text{uv}}$ , ranging from 1 to 100. For a wide range of optical depths, very similar emission spectra in the far-infrared are produced. However, because the power-law continuum is observable in the ultraviolet in many Seyferts,  $\tau_{\text{uv}}$  along the line of sight cannot be  $\gg 1$  in general. Fig. 3(c) shows a comparison of a model with  $n(r) \propto r^{-1}$ ,  $\tau_{\text{uv}} = 1$  ( $A_v = 0.23$ ) and  $r_1/r_2 = 0.0055$  with the 'Seyfert' component adopted above. The fit is satisfactory, though it is clear that the underlying power-law continuum does not extend beyond 100  $\mu\text{m}$ . This is consistent with the turn-over at 80  $\mu\text{m}$  of the far-infrared spectra of Seyferts deduced by Edelson *et al.* (1987).

Although we have assumed spherical symmetry, the far-infrared spectrum would not be very different if the dust were clumped into clouds, whereas the appearance of the galaxy in the ultraviolet to near-infrared would depend critically on whether a cloud lay along the line-of-sight.

In conclusion, the empirical separation of the 12–100  $\mu\text{m}$  spectra of *IRAS* galaxies into three components can be supported by physically plausible models for each of the components.

## 5 Deconvolution into components

Let  $\Delta\nu_i$ ,  $i = 1–4$ , be the effective bandwidths for the *IRAS* 12, 25, 60 and 100  $\mu\text{m}$  bands (i.e. 13.48, 5.16, 2.58 and  $1.00 \times 10^{12}$  Hz, respectively, *IRAS Explanatory Supplement* 1984) and suppose  $S_i$  are the fluxes in Jy in each band for a particular galaxy. Let

$$S_{\text{tot}} = \sum_{i=1}^4 S_i \Delta \nu_i \quad (1)$$

and

$$y_i = S_i / S_{\text{tot}}, \quad i = 1-4. \quad (2)$$

For the 'disc' component ( $j = 1$ ), 'starburst' component ( $j = 2$ ) and 'Seyfert' component ( $j = 3$ ), let the flux in band  $i$  be  $T_{j,i}$  (Jy) and let

$$T_{j,\text{tot}} = \sum_{i=1}^4 T_{j,i} \Delta \nu_i \quad (3)$$

$$t_{j,i} = T_{j,i} / T_{j,\text{tot}}. \quad (4)$$

We then look for the least-squares solution of the over-determined set of equations

$$y_i = \sum_{j=1}^3 \alpha_j t_{j,i}, \quad i = 1-4, \quad (5)$$

to determine the relative proportions,  $\alpha_j$ ,  $j = 1-3$ , of the spectrum attributable to component  $j$ . If any of the  $\alpha_j$  are found to be negative, the most negative is set to zero and the equations re-solved with one fewer variable. If one of the  $\alpha_j$  is still negative, the remaining one is set to be 1. Table 2 gives the resulting values of  $\alpha_j$  for each galaxy, together with the rms deviation of the observed normalized spectrum from the best-fitting mixture,  $\sigma$ . For more than 90 per cent of the galaxies,  $\sigma \leq 0.05$ , indicating an excellent fit of the synthesized spectra to those observed. The final selection of the locations D, B, S in Figs 1(a) and (b) was made after some dozens of runs, to give the best distribution of  $\sigma$ . The solution is stable in the sense that small changes in the choice of component spectra lead to correspondingly small changes in the  $\alpha_j$ . We estimate that the uncertainty in the values of the  $\alpha_j$  is  $\pm 0.05$  and that values of  $\alpha_j$  smaller than 0.05 are not meaningful, since the effect on the *IRAS* colours would be smaller than the uncertainty in these colours (typically 5–10 per cent), and these values are shown bracketed.

We have also investigated the effect of introducing a fourth, 'quasar' component, with a power-law spectrum from 12–100  $\mu\text{m}$ , with spectral index  $\alpha = 0.7$  (broken curve in Fig. 2). The first iteration of equation (5) then becomes a pure matrix inversion, but if some  $\alpha_j$  are negative, then the most negative is set to zero and the second iteration is a least-squares solution, as before. Poor fits with a three-component model ( $\sigma > 0.05$ ) were improved to good fits for only three sources, namely the quasar 3C 273 and the Seyfert 1 galaxies NGC 3516 and Mkn 509. The three-component model of section 4 gives a better fit to the overall spectra of the latter two galaxies and probably also for 3C 273 (see Fig. 9c), so we have not included this fourth component in the analysis described below.

Table 3 summarizes the number of each mixture combination for each galaxy type. All Seyferts but one have a 'starburst' component and all but four have an infrared 'Seyfert' component. It is possible that the narrow-line regions of these latter Seyferts are deficient in dust. We can be reasonably confident that galaxies in which more, than, say, 20 per cent of the far-infrared light is contributed by the 'Seyfert' component do indeed have Seyfert nuclei, though the dust extinction may obscure this Seyfert nucleus at visible wavelengths in some cases. Spectroscopy undertaken subsequent to our model-fitting work has confirmed that 03344-2103, 10140-3318, 13035-4008 and 20243-0226 are Seyferts.

## 6 Relationships between luminosities in components

We now test the consistency of our models by investigating the relationship between the luminosities of the different components. To calculate the far-infrared luminosities in each

Table 2. Parameters for three-component model for galaxies of Table 1.

IRAS name	$\alpha_1$	$\alpha_2$	$\alpha_3$	$\sigma$	$\lg L_{\text{opt}}$	$\lg L_{\text{D}}$	$\lg L_{\text{B}}$	$\lg L_{\text{S}}$
						( $L_{\odot}$ )		
00014+2028	0.910	0.008	0.084	0.010	11.06	10.55	9.29	9.52
00073+2538	0.472	0.545	-	0.017	10.92	10.95	11.01	9.98
00344-3349	-	0.750	0.286	0.063	10.66	10.09	11.27	10.85
00345-2945	0.456	0.583	-	0.031	10.27	10.74	10.84	9.78
00362+5819	0.560	0.445	0.003	0.047	9.56	10.48	10.38	9.03
00506+7248	0.202	0.807	-	0.006	9.66	10.97	11.57	10.36
00509+1225	0.137	0.177	0.691	0.025	11.78	11.23	11.34	11.93
01091-3820	0.069	-	0.948	0.083	10.22	9.55	9.41	10.69
01219+0331	0.413	0.677	-	0.069	10.59	10.72	10.93	9.80
01384-7515	0.497	0.532	-	0.023	-	10.68	10.71	9.68
01403+1323	0.412	0.653	-	0.050	10.11	10.32	10.52	9.41
01484+2220	0.462	0.558	-	0.038	11.30	11.52	11.60	10.55
02069-2339	0.840	-	0.165	0.020	-	10.99	9.76	10.28
02071+3857	0.748	0.260	-	0.016	11.05	11.42	10.96	10.24
02080+3725	0.610	0.399	-	0.012	10.91	10.93	10.75	9.85
02140-1134	0.602	0.367	0.035	0.025	10.62	10.75	10.54	9.76
02208+4744	0.375	0.669	-	0.034	10.31	11.06	11.13	10.08
02252+3105	0.341	0.059	0.606	0.034	10.81	10.59	9.82	10.84
02345+2053	0.434	0.583	-	0.025	10.69	10.85	10.97	9.91
02360-0653	0.226	0.792	-	0.013	10.09	9.93	10.48	9.28
02398+2821	0.665	0.354	-	0.024	9.27	9.37	9.10	8.25
02401-0013	0.193	0.233	0.579	0.029	10.95	10.82	10.90	11.30
02435+1253	0.616	0.431	-	0.043	10.26	11.26	11.11	10.17
02509+1248	0.585	0.438	-	0.027	10.87	10.81	10.69	9.75
02568+3637	0.118	0.821	0.059	0.018	10.51	10.19	11.03	9.89
03064-0308	0.128	0.879	-	0.007	9.91	10.00	10.83	9.59
03117+4157	0.266	0.697	0.040	0.014	11.08	11.02	11.44	10.29
03164+4118	0.021	0.471	0.503	0.037	11.40	10.13	11.11	11.14
03220-3631	0.487	0.573	-	0.046	10.42	9.87	9.94	8.88
03222-0319	0.083	0.435	0.479	0.019	10.10	9.35	10.07	10.11
03266+4138	0.661	0.159	0.193	0.082	10.49	10.81	10.19	10.27
03315+6723	0.666	0.301	0.038	0.031	-	10.56	10.21	9.44
03317-3619	0.464	0.561	-	0.022	10.94	10.86	10.94	9.89
03344-2103	-	0.841	0.179	0.022	9.33	8.78	10.00	9.33
03348-3609	0.328	0.480	0.192	0.004	10.23	9.65	9.81	9.41
03406+3908	0.560	0.397	0.052	0.052	10.98	10.82	10.67	9.79
03451+6956	0.177	0.849	-	0.022	9.28	10.08	10.76	9.53
03514+1546	0.211	0.798	0.002	0.068	10.65	10.67	11.25	10.05
03524-2038	0.312	0.698	-	0.015	9.41	10.31	10.66	9.51
04097+0525	0.576	0.436	-	0.033	9.98	11.10	10.98	10.04
04118-3207	0.325	0.695	-	0.019	9.84	10.65	10.98	9.84
04315-0840	-	0.961	0.046	0.014	10.57	10.48	11.77	10.48
04326+1904	0.612	0.380	0.011	0.009	10.47	11.33	11.12	10.24
04339-1028	0.281	0.364	0.361	0.038	10.69	10.99	11.11	11.10
04370-2416	0.543	0.468	-	0.025	10.39	10.74	10.67	9.70
05053-0805	0.251	0.785	-	0.027	10.01	10.53	11.03	9.83
05054+1718	0.288	0.754	-	0.033	10.60	10.86	11.28	10.10
05368+4940	0.502	0.598	-	0.077	11.15	11.27	11.35	10.27
05445-1648	0.980	-	0.020	0.027	9.77	10.55	9.26	9.26
05497-0728	0.281	0.551	0.175	0.040	10.31	9.75	10.04	9.54
05511+4625	0.148	0.186	0.658	0.049	11.30	10.43	10.53	11.08
05562-6933	0.462	0.539	0.004	0.026	-	10.58	10.65	9.61
06097+7103	-	0.349	0.659	0.059	10.58	9.73	10.57	10.85
06140+8220	0.415	0.524	0.067	0.040	10.38	10.55	10.65	9.76
06259-4708	0.190	0.840	-	0.022	11.02	11.31	11.95	10.73
06456+6054	0.320	0.551	0.129	0.001	10.40	9.94	10.17	9.54
06584+0158	0.451	0.584	-	0.029	8.74	10.08	10.19	9.12
07054+1851	0.454	0.612	-	0.051	10.63	10.58	10.71	9.63
07077-2729	0.269	0.748	-	0.014	-	10.40	10.84	9.67
07107+3521	0.233	0.405	0.366	0.024	10.28	10.11	10.35	10.31
07145-2914	0.103	0.542	0.347	0.051	9.41	8.99	9.71	9.52
07160-6215	0.544	0.503	-	0.037	10.71	10.94	10.91	9.90
07202-2908	0.461	0.576	-	0.029	-	10.50	10.60	9.54
07203+5803	0.723	0.176	0.103	0.012	10.73	10.48	9.87	9.64
07256+3355	0.304	0.754	-	0.044	10.11	10.80	11.20	10.02

Table 2 – continued

07336+3521	0.419	0.610	-	0.032	10.68	10.65	10.81	<	9.72
07388+4955	0.198	0.210	0.594	0.007	10.91	10.30	10.33		10.78
08014+0515	-	0.140	0.868	0.069	10.20	<	9.46		10.70
08171-2501	-	0.217	0.783	0.027	-	<	8.74		9.93
08341-2614	-	0.893	0.103	0.030	9.14	<	8.54		8.86
08425+7416	0.397	0.626	-	0.017	10.24	10.47	10.67	<	9.57
08437-1907	0.314	0.655	0.032	0.006	9.85	9.57	9.89	<	8.78
09108+4019	0.356	0.595	0.051	0.008	10.56	10.25	10.47		9.41
09120+4107	0.526	0.481	-	0.016	9.69	10.50	10.47	<	9.48
09122-6034	0.185	0.827	-	0.009	7.10	10.12	10.77	<	9.55
09141+4212	0.214	0.831	-	0.035	9.96	10.05	10.64	<	9.42
09320+6134	0.475	0.611	-	0.066	10.71	11.85	11.96	<	10.87
09394+0033	0.899	0.079	0.023	0.004	10.31	10.30	9.24	<	9.04
09399+3204	0.588	0.429	-	0.016	10.03	10.01	9.88	<	8.94
09479+3347	0.750	0.147	0.104	0.009	9.76	9.87	9.16		9.01
09511+0148	0.631	0.386	0.000	0.013	9.95	9.86	9.65	<	8.76
09554+3236	0.624	0.348	0.034	0.035	9.91	10.05	9.79	<	8.95
09578-3118	0.661	0.369	-	0.023	10.55	10.51	10.26	<	9.39
09586+1600	0.175	0.609	0.218	0.012	10.04	10.03	10.57		10.13
10015-0614	0.593	0.433	-	0.025	10.66	11.11	10.97	<	10.03
10039-3338	0.047	1.006	-	-	-	<	10.54		10.54
10138+2122	0.561	0.450	-	0.017	9.50	9.78	9.69	<	8.73
10140-3318	0.349	0.382	0.275	0.032	10.01	9.97	10.01		9.87
10257-4338	0.186	0.843	-	0.022	10.90	10.99	11.64	<	10.42
10292-4148	0.631	0.183	0.193	0.044	-	10.90	10.36		10.38
10293-3941	0.670	0.317	0.018	0.029	-	10.51	10.18	<	9.38
10295-3435	0.088	0.493	0.421	0.004	10.71	9.83	10.58		10.51
10356+5345	0.203	0.835	-	0.030	10.17	9.78	10.40	<	9.17
10409-4557	0.692	0.297	0.013	0.009	-	11.31	10.94	<	10.17
10439+1400	0.574	0.331	0.094	0.009	10.69	10.48	10.24		9.70
10489+3309	0.569	0.460	-	0.027	9.85	9.99	9.90	<	8.93
10560+6147	0.286	0.746	-	0.024	10.20	9.99	10.41	<	9.23
10570+5110	0.230	0.554	0.223	0.038	9.89	9.85	10.23		9.83
11004+2814	0.361	0.590	0.046	0.017	10.22	10.16	10.37	<	9.30
11005-1601	0.550	0.470	-	0.015	10.12	10.61	10.54	<	9.57
11033+7250	0.192	0.132	0.684	0.050	10.52	9.60	9.43		10.15
11083-4849	0.462	0.525	0.018	0.033	10.35	10.27	10.33	<	9.30
11113+4835	0.795	0.186	0.022	0.016	10.44	10.46	9.82	<	9.25
11119+1305	0.539	0.464	0.003	0.043	9.46	9.45	9.38	<	8.41
11122-2327	0.218	0.801	-	0.020	10.45	10.35	10.92	<	9.71
11143-7556	0.381	0.713	-	0.071	-	-	-	-	-
11186-0242	0.416	0.578	0.011	0.028	10.78	11.02	11.17	<	10.10
11202+1651	0.779	0.216	0.008	0.011	9.99	10.06	9.50	<	8.87
11247+5709	0.639	0.348	0.019	0.038	9.83	10.44	10.18	<	9.34
11330+7048	0.739	0.177	0.088	0.019	10.68	10.68	10.06		9.75
11365-3727	0.131	0.183	0.680	0.044	10.71	9.77	9.92		10.49
11442-2738	0.265	0.768	-	0.033	9.91	9.85	10.31	<	9.13
11449+5614	0.724	0.260	0.022	0.032	10.18	10.36	9.92	<	9.20
11506-3851	0.323	0.808	-	0.101	-	10.79	11.19	<	9.98
12002+4854	0.867	0.043	0.095	0.028	10.44	10.65	<	9.41	9.69
12038+5259	0.287	0.757	-	0.035	9.70	10.03	10.45	<	9.27
12116+5448	0.069	0.937	-	0.007	10.30	9.95	11.08	<	9.81
12131+3636	0.463	0.597	-	0.050	9.51	8.73	8.84	<	7.76
12159+3005	0.026	0.643	0.331	0.004	10.37	<	9.51	10.62	10.33
12173+0537	0.644	0.364	-	0.007	10.38	10.47	10.23	<	9.37
12232+1256	0.252	0.475	0.268	0.036	10.05	9.51	9.78		9.53
12243-0036	-	1.000	-	0.051	9.82	<	9.84	11.14	< 9.84
12244+1519	0.592	0.326	0.079	0.021	9.97	9.71	9.45		8.84
12250-0800	0.566	0.472	-	0.029	10.38	10.71	10.63	<	9.66
12265+0219	0.266	0.113	0.633	0.078	12.88	12.38	12.01		12.75
12290+5814	0.410	0.496	0.098	0.022	10.40	10.20	10.28		9.57
12329-3938	0.124	0.576	0.302	0.003	10.69	9.81	10.48		10.20
12381-3628	0.222	0.505	0.268	0.030	9.98	10.22	10.58		10.30
12412+1639	0.938	0.066	-	0.006	10.12	9.74	8.59	<	8.47
12456-0303	0.267	0.741	-	0.008	9.90	9.53	9.97	<	8.80
12483+7308	0.979	-	0.021	0.004	10.17	10.16	<	8.87	< 8.87
12493+7154	0.802	0.210	-	0.016	9.76	10.14	9.56	<	8.94
12517-1015	0.734	0.279	-	0.026	9.75	9.49	9.07	<	8.33

Table 2 – *continued*

12522+2912	0.746	0.274	-	0.015	10.53	10.72	10.29	<	9.55
12523+4648	0.901	0.101	-	0.002	9.52	9.53	8.58	<	8.28
12532+0434	0.700	0.204	0.107	0.062	9.31	9.36	8.82		8.54
12540+5708	-	0.882	0.128	0.015	11.13	< 11.39	12.63		11.80
12540-0717	0.586	0.436	-	0.031	9.07	9.56	9.43	<	8.49
12542-0815	0.164	0.832	0.003	0.011	9.97	9.46	10.17	<	8.94
12554+0150	0.831	0.218	-	0.038	9.97	9.98	9.40	<	8.76
12580+0246	0.706	0.314	-	0.024	9.69	9.51	9.16	<	8.36
13035-4008	0.379	0.341	0.288	0.051	-	10.63	10.58		10.51
13062-1514	0.277	0.690	0.040	0.041	10.03	9.52	9.92	<	8.78
13099-1716	0.736	0.224	0.046	0.033	10.63	10.54	10.03	<	9.38
13136+6223	-	1.000	-	0.019	10.98	< 10.62	11.92	<	10.62
13142-1622	0.784	0.244	-	0.022	10.50	10.34	9.84	<	9.15
13170-2708	1.000	-	-	0.028	10.36	10.64	< 9.34	<	9.34
13197-1627	0.018	0.450	0.530	0.016	10.38	< 9.95	10.90		10.97
13229-2934	0.480	0.537	-	0.022	10.80	11.05	11.09	<	10.06
13230+4331	0.572	0.445	-	0.029	9.47	9.75	9.65	<	8.70
13286-3432	0.374	0.677	-	0.039	10.34	10.50	10.76	<	9.63
13301-2357	0.596	0.383	0.025	0.026	10.65	10.89	10.70	<	9.82
13304+6301	0.554	0.467	-	0.017	10.37	10.54	10.46	<	9.49
13370-3123	-	0.681	0.326	0.038	9.18	< 8.02	9.16		8.84
13373+0105	0.474	0.538	-	0.016	10.91	11.30	11.35	<	10.32
13464-3003	0.028	-	0.978	0.032	10.48	< 9.75	< 9.75		11.05
13477-4848	0.464	0.554	-	0.016	10.97	10.74	10.82	<	9.78
13510+3344	0.249	0.115	0.631	0.030	10.00	9.56	9.22		9.96
13536+1836	0.006	0.220	0.774	0.001	11.20	< 10.66	11.31		11.85
13550+4205	0.723	0.264	0.013	0.003	10.51	10.34	9.90	<	9.18
13591+5934	0.496	0.506	-	0.012	10.47	10.64	10.65	<	9.64
14045+5057	0.815	0.162	0.023	0.001	10.04	10.08	9.38	<	8.87
14092-6506	0.137	0.667	0.195	0.012	9.66	9.19	9.88		9.34
14106-0258	0.082	0.443	0.477	0.007	9.93	9.40	10.14		10.17
14152-4309	0.979	-	0.019	0.016	10.01	9.66	< 8.37	<	8.37
14179-4604	0.497	0.520	-	0.018	-	10.00	10.02	<	9.00
14188+7148	0.315	0.608	0.083	0.034	10.94	10.92	11.20		10.34
14214+1451	0.614	0.373	0.019	0.037	10.04	10.27	10.05	<	9.18
14280+3126	0.542	0.434	0.030	0.032	10.56	10.88	10.78	<	9.84
14283+3532	0.872	0.019	0.114	0.030	10.56	10.43	< 9.19		9.55
14299+0817	0.563	0.443	-	0.016	10.25	10.26	10.15	<	9.20
14349+5900	0.010	0.409	0.579	0.017	10.91	< 10.18	11.09		11.24
14351+0230	0.814	0.209	-	0.021	10.23	10.19	9.60	<	8.98
14383-0006	0.634	0.370	0.003	0.040	9.81	10.14	9.91	<	9.04
14454-4343	0.073	0.548	0.378	0.011	11.13	10.73	11.61		11.45
14483+0519	0.325	0.483	0.193	0.002	10.78	10.92	11.09		10.69
14544-4255	0.418	0.578	0.002	0.017	-	10.88	11.02	<	9.96
14556-4148	0.865	0.117	0.014	0.028	-	10.61	9.75	<	9.38
15005+8343	0.299	0.644	0.060	0.017	10.53	10.39	10.72		9.69
15187-1254	0.335	0.703	-	0.031	10.36	10.17	10.49	<	9.34
15243+4150	0.253	0.756	-	0.008	10.30	10.18	10.66	<	9.48
15276+1309	0.479	0.525	-	0.004	10.64	10.82	10.86	<	9.84
15437+0234	0.351	0.591	0.061	0.015	10.83	10.68	10.91		9.92
15456-1336	0.428	0.321	0.255	0.028	10.75	11.01	10.88		10.87
15467-2914	0.391	0.652	-	0.034	10.25	10.70	10.92	<	9.80
15496+4724	0.826	0.053	0.125	0.030	10.88	11.13	9.94		10.31
16104+5235	0.292	0.666	0.043	0.003	11.08	11.15	11.51	<	10.39
16180+3753	0.570	0.398	0.036	0.024	10.93	11.31	11.15	<	10.25
16301+1955	0.682	0.330	-	0.009	10.56	10.58	10.26	<	9.44
16504+0228	0.103	0.953	-	0.043	10.77	11.04	12.00	<	10.72
17366+8646	0.636	0.354	0.014	0.022	10.86	11.26	11.00	<	10.15
17530+3446	0.663	0.341	-	0.005	10.69	11.00	10.71	<	9.88
18001+6638	-	0.657	0.336	0.042	9.89	< 9.15	10.27		9.97
18097-6006	0.373	0.539	0.091	0.014	-	10.28	10.44		9.67
18095+1458	0.551	0.451	0.003	0.030	10.60	10.67	10.59	<	9.63
18329+5950	0.452	0.577	-	0.023	10.64	11.49	11.60	<	10.14
18341-5732	0.540	0.539	-	0.061	-	11.12	11.12	<	9.68
18401-6225	0.217	0.206	0.585	0.048	10.10	10.02	10.00		10.45
19070+5051	0.392	0.538	0.067	0.024	10.37	10.25	10.39		9.48
19385-7045	0.784	0.130	0.090	0.023	10.49	10.82	10.04		9.88
19393-5846	0.444	0.498	0.055	0.022	10.38	10.37	10.42		9.46

Table 2 – continued

19414+4510	0.536	0.512	-	0.038	9.74	9.66	9.64	<	8.23
19517-1241	0.330	0.693	-	0.020	10.10	9.98	10.30	<	9.16
19582-3833	0.612	0.120	0.283	0.098	-	10.79	10.08	10.45	
20243-0226	0.185	0.006	0.810	0.006	10.61	10.55	<	9.59	11.19
20264+2533	0.438	0.598	-	0.042	10.65	10.94	11.08	<	10.00
20727-4738	0.278	0.759	-	0.028	-	9.86	10.30	<	9.12
20414-1054	0.122	0.197	0.689	0.052	11.61	10.48	10.69		11.23
20481-5715	-	0.339	0.673	0.029	10.52	<	9.71	10.54	10.84
20551-4250	-	1.000	-	0.044	11.18	<	10.89	12.19	< 10.89
21193-3653	0.420	0.614	-	0.031	-	10.30	10.46	<	9.37
21453-3511	0.374	0.665	-	0.030	10.77	11.10	11.35	<	10.22
21591-3206	0.622	0.321	0.061	0.024	10.38	10.43	10.15		9.43
22132-3705	0.548	0.467	-	0.020	10.74	11.07	11.00	<	10.03
23007+0836	0.163	0.797	0.039	0.009	11.04	11.01	11.70	<	10.50
23121+0415	0.690	0.351	-	0.032	10.70	10.98	10.69	<	9.84
23128-5919	-	1.000	-	0.039	11.05	<	10.86	12.16	< 10.86
23134-4251	0.239	0.778	-	0.012	10.49	10.60	11.11	<	9.92
23135+2516	0.157	0.862	-	0.016	10.58	10.97	11.70	<	10.47
23156-4238	0.337	0.718	-	0.043	10.42	10.43	10.76	<	9.60
23179+1657	0.605	0.400	-	0.017	10.05	10.26	10.08	<	9.18
23179+2702	0.873	0.023	0.108	0.032	10.42	10.84	<	9.60	9.94
23259+2208	0.595	0.413	-	0.008	10.68	10.75	10.59	<	9.67
23260-4136	1.000	-	-	0.023	9.96	10.03	<	8.73	< 8.73
23262+0314	0.261	0.678	0.070	0.048	10.81	10.70	11.11		10.12
23488+1949	0.664	0.390	-	0.043	10.80	11.35	11.12	<	10.22
23488+2018	0.176	0.870	-	0.035	10.66	11.23	11.92	<	10.68

Table 3. Numbers of galaxies with different combinations of ‘disc’ (D), ‘starburst’ (B) and ‘Seyfert’ (S) components

Type	Number	
D	5	(NGC 2076, 4750, 5078, 5530; 23260-4136)
B	6	(NGC 1614, 4418; UGC 8335; 10039-3338, 20551-4250, 23128-5919)
S	1	(IC 4329A)
DB	138	
DBS	55	
DS	7	(NGC 4047, 5656, 7624, 7817; 01091-3820, 02069-2339, 20243-0226)
BS	15	(NGC 1275, 1377, 4253, 5253, 6552; UGC 3426, 4203, 8058, 8850, 9412; 00344-3349, 08171-2501, 08341-2614, 13197-1627, 20481-5715)

component we need to apply a correction for the incomplete wavelength coverage of the *IRAS* bands. Lonsdale *et al.* (1984) have shown that the quantity  $1.26(S_3\Delta\nu_3 + S_4\Delta\nu_4)$  is an excellent approximation to the 42.5–122.5  $\mu\text{m}$  integrated spectrum of sources with blackbody or power-law spectra. Although the great variety of spectral behaviour over the wider range 10–100  $\mu\text{m}$  makes it impossible to achieve as good a result over this whole wavelength range, the quantity

$$1.26S_{\text{tot}} = 1.26 \sum_{i=1}^4 S_i \Delta\nu_i \quad (6)$$

is a good approximation to the integrated spectrum from 10–120  $\mu\text{m}$  of the ‘Seyfert’ component model adopted here and is within 15 per cent for the ‘starburst’ model, so we adopt this as a measure of the 10–120  $\mu\text{m}$  far-infrared flux from galaxies.

We have then calculated luminosities in each component, using

$$L_j = 1.26 \alpha_j S_{\text{tot}} \times 4\pi d^2, \quad (7)$$

where  $d$  is the luminosity distance calculated in an  $\Omega = 1$  universe for  $H = 50 \text{ km s}^{-1} \text{ Mpc}^{-1}$ . These are listed in Table 2. Where  $\alpha_j \leq 0.05$ , upper limits have been given based on  $\alpha_j = 0.05$ . We have also calculated optical luminosities based on  $\nu S_\nu$  in the  $B$ -band, applying the de Vaucouleurs *et al.* (1976) internal extinction correction. Corrections for interstellar extinction have been derived from the maps of Burstein & Heiles (1978), assuming  $A_B = 4E(B-V)$ . Optical luminosities have not been quoted for galaxies with  $b < 10^\circ$  unless direct estimates of interstellar extinction are available. Zwicky magnitudes were corrected according to the formula adopted by Rowan-Robinson, Helou & Walker (1987) for  $m_Z \leq 14.5$  and using the corrections of Kron & Shane (1976) for  $m_Z > 14.5$ . Also given is the total far-infrared (10–120  $\mu\text{m}$ ) luminosity based on equation (6).

Fig. 4 shows the relationship between  $L_D$ , the luminosity in the ‘disc’ component, and  $L_{\text{opt}}$ , the luminosity in the blue band (known Seyferts and galaxies for which the proportion of the far-infrared luminosity in the form of a Seyfert component,  $\alpha_3$ , is greater than 20 per cent, have been excluded). Fig. 5 shows the relationship between  $L_B$ , the luminosity in the ‘starburst’ component, and  $L_{\text{opt}}$ , and Fig. 6 shows the distribution of  $L_D/L_{\text{opt}}$  versus  $L_B/L_{\text{opt}}$ . Table 4 gives the mean values of  $\log(L_D/L_{\text{opt}})$  and  $\log(L_B/L_{\text{opt}})$ , and their dispersion, for different categories of galaxies.

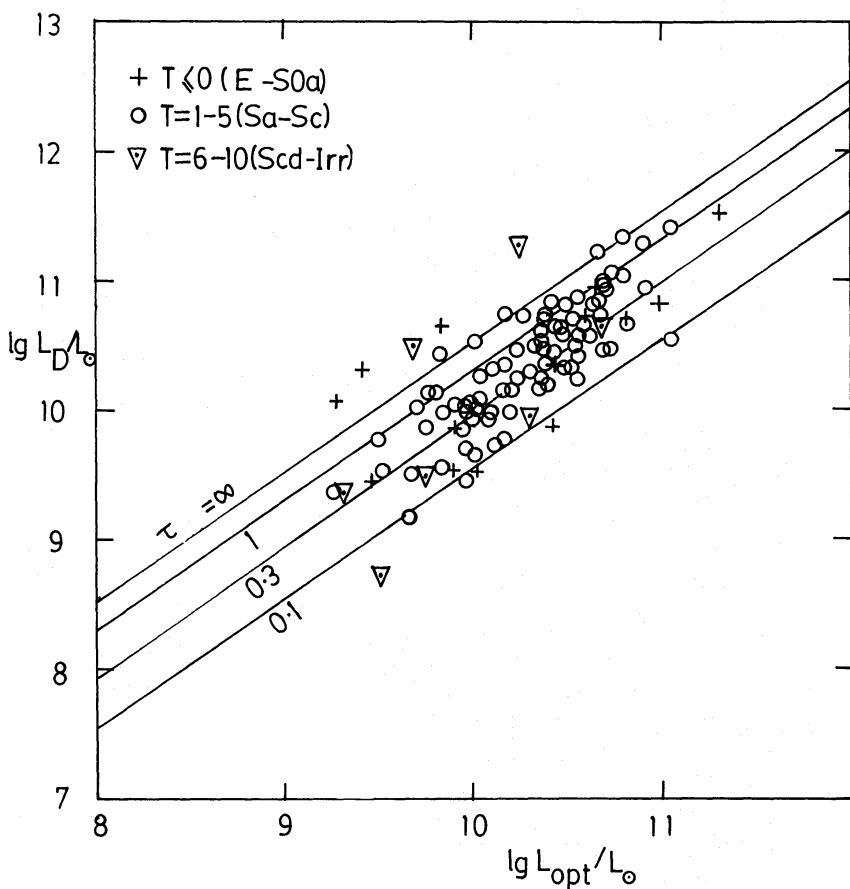


**Figure 4.** The correlation of the luminosity in the ‘disc’ component,  $L_D$ , in solar units, versus the blue luminosity of the galaxy.  $H_0 = 50 \text{ km s}^{-1} \text{ Mpc}^{-1}$ , and  $\Omega_0 = 1$ , throughout this paper. Different symbols are used for different ranges of galaxy types, based on the parameter  $T$  of de Vaucouleurs *et al.* (1976): + E-S0a,  $\circ$  Sa-Sbc,  $\nabla$  Sd-Irr. Seyfert galaxies have been excluded from this figure. The solid lines give values of the characteristic optical depth  $\tau$  derived from equation (8).

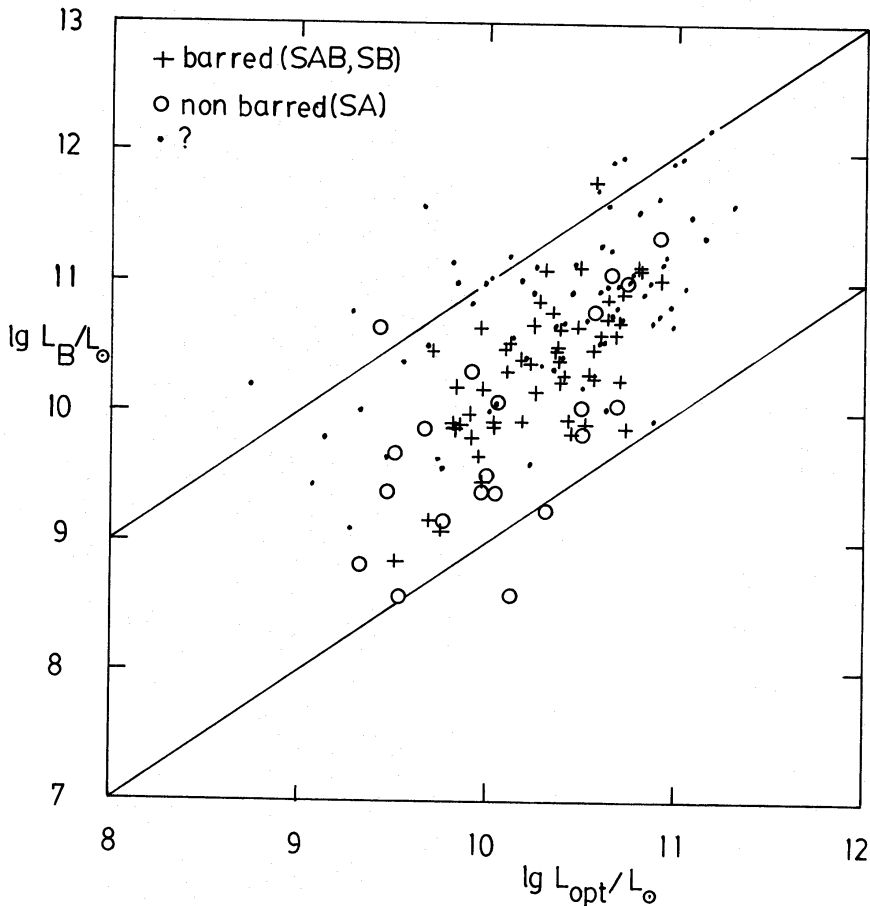


**Figure 5.** The correlation of the luminosity in the ‘starburst’ component,  $L_B$ , in solar units, versus the blue luminosity of the galaxy. The symbols denote: + barred galaxies (SB or SAB),  $\odot$  un-barred galaxies (SA), · bar-type unknown or not relevant. Seyfert galaxies have been excluded from this figure. The solid sloping lines correspond to galaxies in which the luminosity in the starburst component is 10 times (upper) and 0.1 times (lower) the optical luminosity.

From Figs 4–6 and Table 4 we can draw a number of conclusions:

- (i) For non-Seyfert galaxies with  $L_B/L_{\text{opt}} < 4$ , there is a tight correlation of  $L_D$  with  $L_{\text{opt}}$ . If the ‘disc’ component is interpreted as emission from interstellar dust as a result of absorption of starlight, then the ratio  $L_D/L_{\text{opt}}$  can be interpreted in terms of a characteristic optical depth in dust

$$L_D/L_{\text{opt,tot}} = 1 - \exp(-\tau), \quad (8)$$

where

$$L_{\text{opt,tot}} = \int_{\text{opt-uv}} L_\nu d\nu = 3.3 L_{\text{opt}}$$

by integration over the interstellar radiation field model of Mathis, Mezger & Panagia (1983). Lines of constant  $\tau$ , as given by equation (8), are indicated in Figs 4 and 6. For almost all galaxies the values of  $\tau$  are consistent with the internal extinction formula of de Vaucouleurs *et al.* (1976) and there is no evidence for exceptionally high internal extinction in these galaxies.

- (ii) For galaxies with  $L_B/L_{\text{opt}} > 4$ , one third of the galaxies have values of  $L_D/L_{\text{opt}} > 3.3$ , inconsistent with equation (8) for any  $\tau$ . It does not seem plausible to attribute all of these to

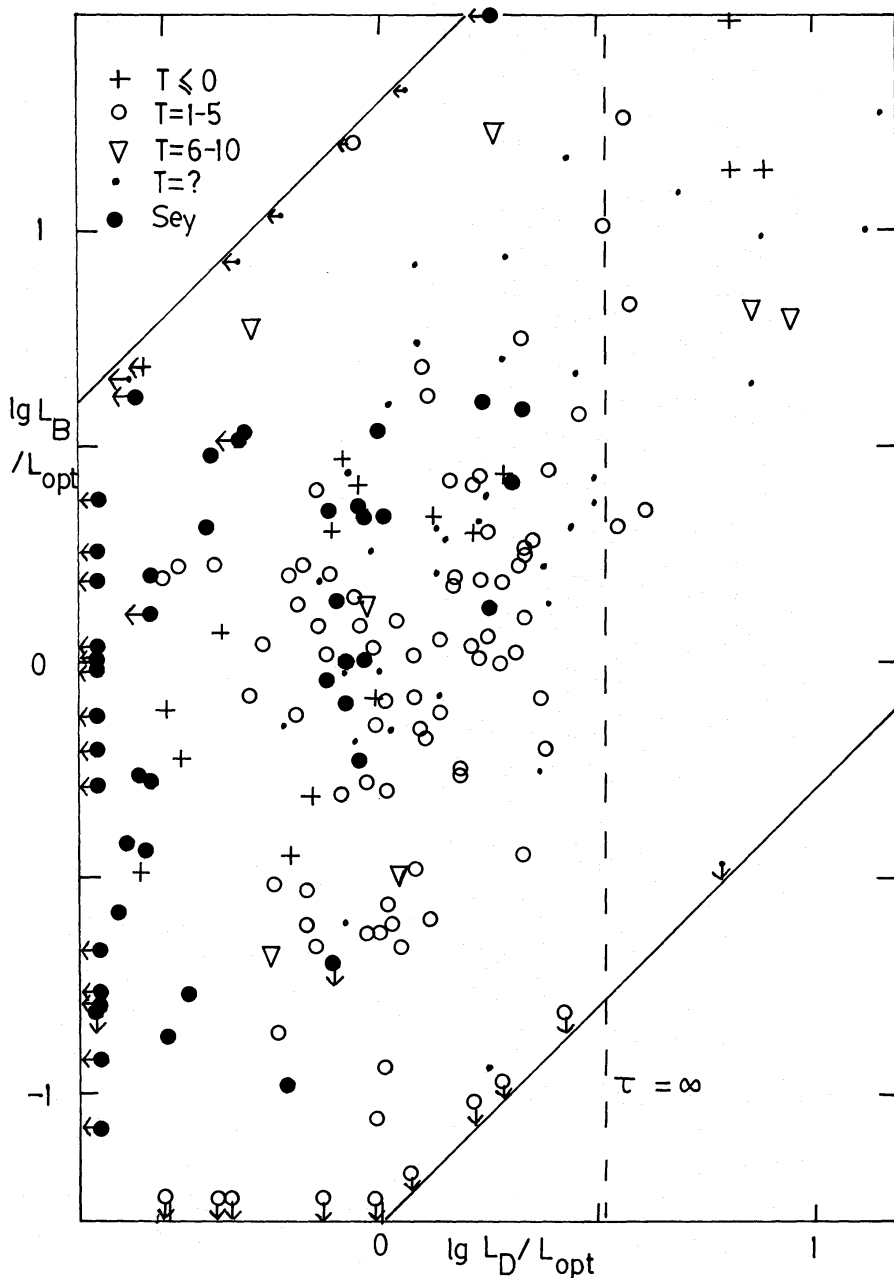


**Figure 6.**  $\log(L_B/L_{\text{opt}})$  versus  $\log(L_D/L_{\text{opt}})$  for IRAS four-band galaxies, with different symbols for different galaxy types: + E-S0a ( $T \leq 0$ ),  $\circ$  Sa-Sc ( $T = 1-5$ ),  $\nabla$  Scd-Irr ( $T = 6-10$ ),  $\bullet$  known Seyferts and galaxies with  $\alpha_3 > 0.2$ , · unknown type. The upper sloping solid lines is the locus of galaxies with  $\alpha_1 = 0.05$ : galaxies with disc components contributing less than 5 per cent of the total 10–120  $\mu\text{m}$  luminosity would lie to the left of this line. The lower sloping solid line is the locus of galaxies with  $\alpha_2 = 0.05$ : galaxies with starburst components contributing less than 5 per cent of the total 10–120  $\mu\text{m}$  luminosity would lie to the right of this line. The vertical broken line corresponds to  $\tau = \infty$  in equation (8).

overestimates of the blue magnitude or to underestimates of the interstellar extinction in our Galaxy. For these galaxies we must conclude either that part of the illumination of the cool ‘disc’ component is provided by the starburst (but without enhancing  $L_{\text{opt}}$ ) or that the internal extinction is considerably higher than that given by the de Vaucouleurs *et al.* formula. The latter was the conclusion of Moorwood, Véron-Cetty & Glass (1986) and de Jong & Brink (1987). These galaxies clearly merit further study.

**Table 4.** Mean values of  $\log(L_D/L_{\text{opt}})$  and  $\log(L_B/L_{\text{opt}})$  as a function of a galaxy type.

Hubble type	$-3 \leq T \leq 0$ S0-S0a	$T = 1$ Sa	2 Sab	3 Sb	4 Sbc	5 Sc	6-10 Scd-Irr	All types*
<i>(a) All galaxies</i>								
$\langle \log(L_D/L_{\text{opt}}) \rangle$	0.09	0.09	0.08	0.15	-0.15	0.05	0.06	0.15
$\sigma$	0.45	0.28	0.27	0.24	0.26	0.21	0.59	0.36
$n$	14	20	14	21	11	19	7	144
$\langle \log(L_B/L_{\text{opt}}) \rangle$	0.39	0.16	0.16	0.07	-0.11	-0.32	0.10	0.18
$\sigma$	0.55	0.10	0.34	0.49	0.33	0.53	0.66	0.57
$n$	15	19	12	20	8	19	7	141
<i>(b) Barred (SAB, SB)</i>								
$\langle \log(L_D/L_{\text{opt}}) \rangle$	-0.39	0.02	0.05	0.08	-0.02	0.06	-0.35	
$\sigma$	0.17	0.28	9.27	0.18	0.22	0.21	-	
$n$	4	12	8	11	5	11	3	
$\langle \log(L_B/L_{\text{opt}}) \rangle$	-0.06	0.18	0.20	0.01	0.03	-0.10	-0.17	
$\sigma$	0.29	0.36	0.20	0.48	0.12	0.44	-	
$n$	4	12	8	11	5	12	3	
<i>(c) Non-barred (SA)</i>								
$\langle \log(L_D/L_{\text{opt}}) \rangle$	0.28	0.27	0.00	0.12	-0.11	-0.06	0.05	
$\sigma$	0.38	-	-	-0.29	0.30	0.16	-	
$n$	4	3	2	6	5	5	1	
$\langle \log(L_B/L_{\text{opt}}) \rangle$	0.50	-0.21	-0.57	0.03	-0.33	-0.87	-0.49	
$\sigma$	0.47	-	-	0.49	-	0.38	-	
$n$	4	2	1	5	3	5	1	

\* Including galaxies of unknown type.

$n$  is number of galaxies,  $\sigma$  is standard deviation, for each bin.

(iii) There is a wide range in values of  $L_B/L_{\text{opt}}$ , consistent with the idea of a transient burst of star formation. Table 4 shows that there is a trend of decreasing  $L_B/L_{\text{opt}}$  with Hubble type from  $T=0-5$  (Sa0-Sc). The highest values of  $L_B/L_{\text{opt}}$  are therefore associated with the galaxies with the most prominent optical nuclei. This is consistent with the finding of Devereux (1987) that early-type spirals have higher S(25)/S(12) than late-type spirals.

(iv) Barred spirals (SAB or SB) have higher values of  $L_B/L_{\text{opt}}$  than non-barred spirals (SA), as reported by Hawarden (1986), but spirals which have not been classified have higher values of  $L_B/L_{\text{opt}}$  than those classified as barred. Since the unclassified galaxies tend to be the more distant ones, this may be merely an effect of Malmquist bias.

(v) The majority of Seyfert galaxies (including galaxies with  $\alpha_3 > 0.2$ ) have exceptionally low values of  $L_D/L_{\text{opt}}$ : 29/48 have  $L_D/L_{\text{opt}} < 0.5$ , compared with 14/150 for non-Seyferts. Why is the cooler ‘disc’ component so weak in many Seyferts? One possibility is that the dust content of these galaxies is exceptionally low because the conditions in the discs of the host galaxies are conducive to efficient transfer of gas and dust to the nucleus. This would be consistent with our finding that almost all our galaxies with ‘Seyfert’ components have accompanying ‘starburst’ components (see also Wilson 1987; Rodrigues-Espinosa 1987). A second possibility is that the enhanced ultraviolet radiation from the Seyfert nucleus raises the grains to a much higher temperature (50 K instead of 25–30 K) so that the contribution of infrared ‘cirrus’ has been included in the warm ‘starburst’ component. This latter explanation does not work for several Seyferts for which both  $L_D/L_{\text{opt}}$  and  $L_B/L_{\text{opt}}$  are low. The enhancement of the galaxy’s blue luminosity by the Seyfert continuum makes some contribution to the lowering of  $L_D/L_{\text{opt}}$ , but is hardly likely to be the major explanation, since only for quasars is the blue light of a galaxy dominated by the nuclear source.

Fig. 7 shows the relationship between  $L_S/L_{\text{opt}}$  and  $L_B/L_{\text{opt}}$  for known Seyferts and galaxies with prominent infrared 'Seyfert' components ( $\alpha_3 > 0.2$ ). No particular correlation is found and the range of values of  $L_B/L_{\text{opt}}$  for Seyferts is similar to that for non-Seyferts (see Fig. 6). The only Seyferts with exceptionally large values of  $L_B/L_{\text{opt}}$  in this sample are Mkn 231 and ESO 148-IG02. It is noticeable that Type 1 Seyferts tend to have higher values of  $L_S/L_B$  than Type 2 and this effect is responsible for the segregation in the *IRAS* colour-colour diagrams noted by Neugebauer *et al.* (1986). This may represent intrinsic differences in the energy sources of Type 1 and Type 2 Seyferts or may be the result of quenching of the compact continuum source in Type 2s by dust (Rowan-Robinson 1977; Lawrence 1987), although it is hard to see how the latter would lead to enhancement of the warm (50  $\mu\text{m}$ ) 'starburst' component at the expense of the hot (25  $\mu\text{m}$ ) 'Seyfert' component.

It is noticeable that Seyferts are limited to values of  $L_S/L_{\text{opt}} < 5$ . This can be understood in terms of a simple model in which a fraction  $f$  of the Seyfert continuum escapes directly, while the remainder,  $(1-f)$ , is subject to absorption by dust with optical depth  $\tau$ . Then, if  $L_{Q,\text{tot}}$  is the total power in the 100  $\mu\text{m}$ -912 Å power-law continuum, assumed to be of the form  $L(\nu) \propto \nu^{-0.7}$ , and  $L_{Q,\text{opt}}$  is the corresponding blue-band luminosity, then

$$L_{Q,\text{tot}}/L_{Q,\text{opt}} = \int_{\nu_{\text{min}}}^{\nu_{\text{max}}} \nu^{-0.7} d\nu / \nu_B^{+0.3} \approx \frac{(\nu_{\text{max}}/\nu_B)^{0.3}}{0.3} \approx 5$$

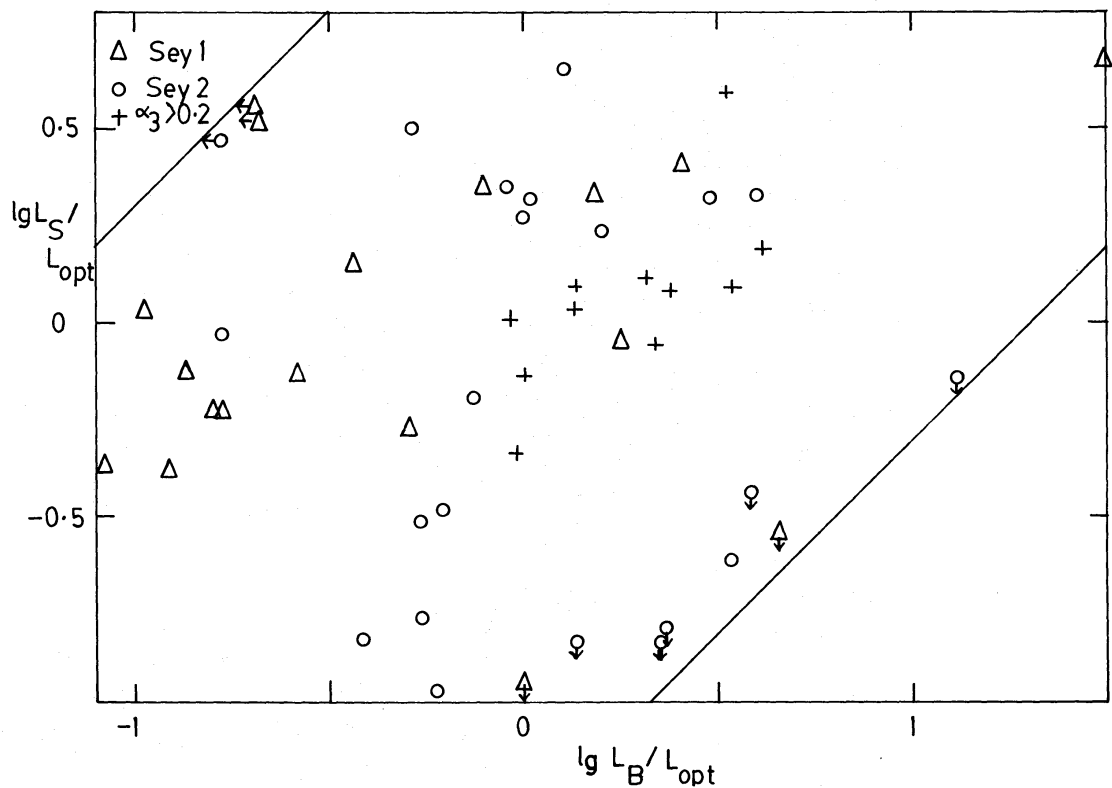


**Figure 7.**  $\log(L_S/L_{\text{opt}})$  versus  $\log(L_B/L_{\text{opt}})$  for known Seyferts ( $\nabla$  Type 1,  $\circ$  Type 2) and for galaxies with  $\alpha_3 > 0.2$  (+). The upper solid sloping line is the locus of galaxies with  $\alpha_2 = 0.05$ : galaxies with starburst components contributing less than 5 per cent of the total 10–120  $\mu\text{m}$  luminosity would lie to the left of this line. The lower sloping solid line is in the locus of galaxies with  $\alpha_3 = 0.05$ : galaxies with 'Seyfert' components contributing less than 5 per cent of the total 1–120  $\mu\text{m}$  luminosity would lie to the right of this line.

and

$$L_S/L_{\text{opt}} = [1 - \exp(-\tau)](1-f) L_{Q,\text{tot}}/L_{\text{opt}} \simeq 5[1 - \exp(-\tau)](1-f) L_{Q,\text{opt}}/L_{\text{opt}} < 5$$

for  $\tau > 0, f < 1, L_{Q,\text{opt}} < L_{\text{opt}}$ .

(Since  $L_{\text{opt}}$  comprises both the galaxy's starlight and the Seyfert continuum  $L_{Q,\text{opt}}/L_{\text{opt}}$  would be  $< 1$  for all cases.)

Fig. 8 shows  $L_S$  versus  $L_X$ , the X-ray luminosity (data from Ward *et al.* 1987; Branduardi-Raymont *et al.* 1981; Lawrence & Elvis 1982; Kriss, Canizares & Ricker 1980; Marshall *et al.* 1979; McHardy *et al.* 1981; Elvis & Lawrence 1989), showing a good correlation, consistent with the idea that the 'Seyfert' component is dust illuminated by the central quasar-like source.  $L_X$  is better correlated with  $L_S$  (correlation coefficient 0.88 for 15 galaxies, excluding the anomalous NGC 1068) than it is with  $L_B$  (correlation coefficient 0.80).

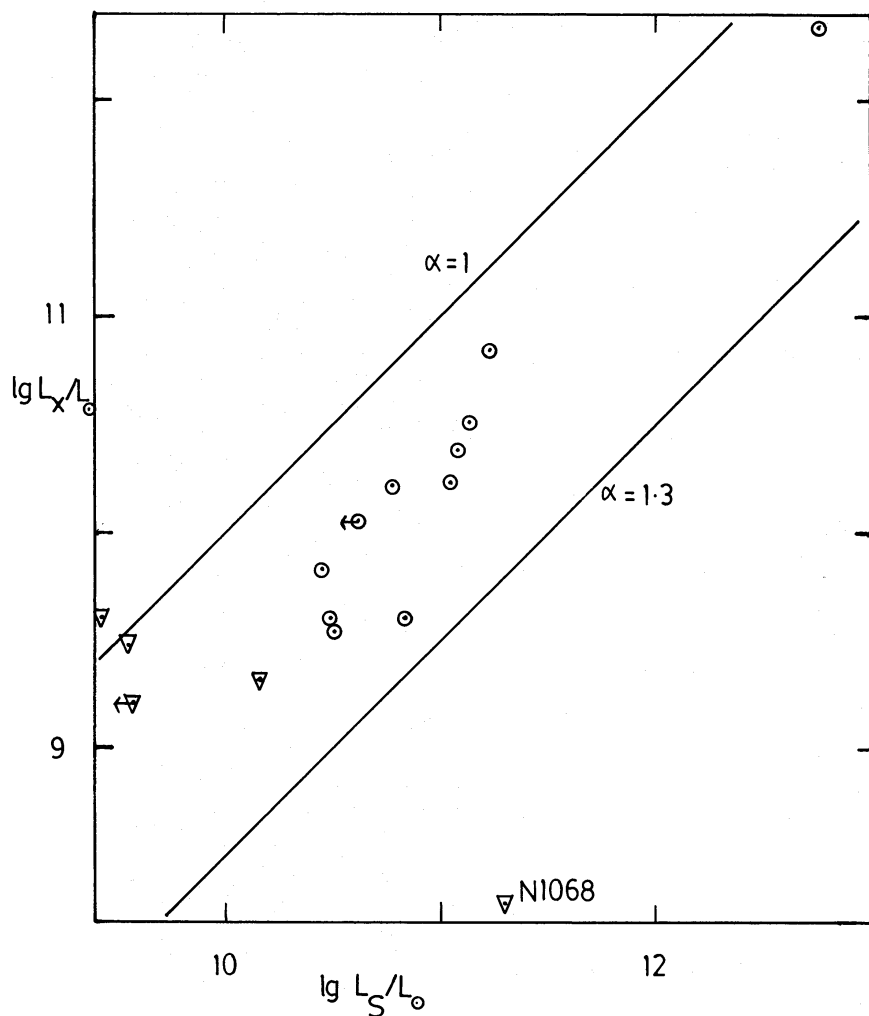


**Figure 8.** The correlation of the 2–10 keV ('hard') X-ray luminosity, in solar units, with the luminosity in the 'Seyfert' component. Seyferts of Type 1 and 2 are denoted by circles and triangles, respectively. The straight lines are labelled with the infrared to X-ray spectral index. X-ray data are from Ward *et al.* (1987), Branduardi-Raymont *et al.* (1981), Lawrence & Elvis (1982), Kriss *et al.* (1980), Marshall *et al.* (1979), McHardy *et al.* (1981), and Elvis & Lawrence (1989).

One worry concerning the model for the disc component was that we may have significantly underestimated the contribution from small grains in the range 12–25  $\mu\text{m}$ . If this were true, however, then it should show up as a correlation between  $L_{\text{D}}$  and  $L_{\text{S}}$ , since the spectrum of the ‘Seyfert’ component peaks in  $\nu S$ , close to where we expect the deficit in the disc luminosity to occur. Any large effect is ruled out by the large scatter in a plot of the two quantities (not shown), and by specific objects where the disc dominates the emission and no ‘Seyfert’ component is present (especially 13170–2708).

Of the 18 galaxies in our sample which have  $L_{\text{IR}} > 3 \times 10^{11} L_{\odot}$ , the far-infrared spectra of 15 are dominated by ‘starburst’ components (including the galaxy NGC 6240, studied by Joseph & Wright 1985; Rieke *et al.* 1985; DePoy, Becklin & Wynn-Williams 1986). The exceptions are the quasar 3C 273, the Seyfert 1 galaxy I Zw 1, and the Seyfert 2 galaxy Mkn 463.

## 7 Model fits to infrared spectra of selected galaxies

For several galaxies in our sample the spectra are known at wavelengths outside the 12–100  $\mu\text{m}$  range studied by *IRAS*, in some cases covering the range from ultraviolet to 1 mm. These spectra provide a strong test of our models. The main conclusion of this comparison is that, while our models give an excellent fit to the infrared spectra of more than 60 per cent of the galaxies with good spectral data, the remainder require modification to give a good fit in the range 1–10  $\mu\text{m}$ . These cases are almost all Seyfert galaxies and the modification required is that the optical depth across the dust cloud in the narrow-line region should be  $\gg 1$ .

There are two other galaxies which require an additional ingredient to bring their predicted spectra into line with observations, namely Arp 220 (not actually in our sample) and NGC 4418. Both have anomalously high  $[\text{S}(25)/\text{S}(12)]$  ratios, most easily understood as being due to heavy extinction by interstellar dust in the parent galaxy.

We now discuss these three classes of galaxy in turn:

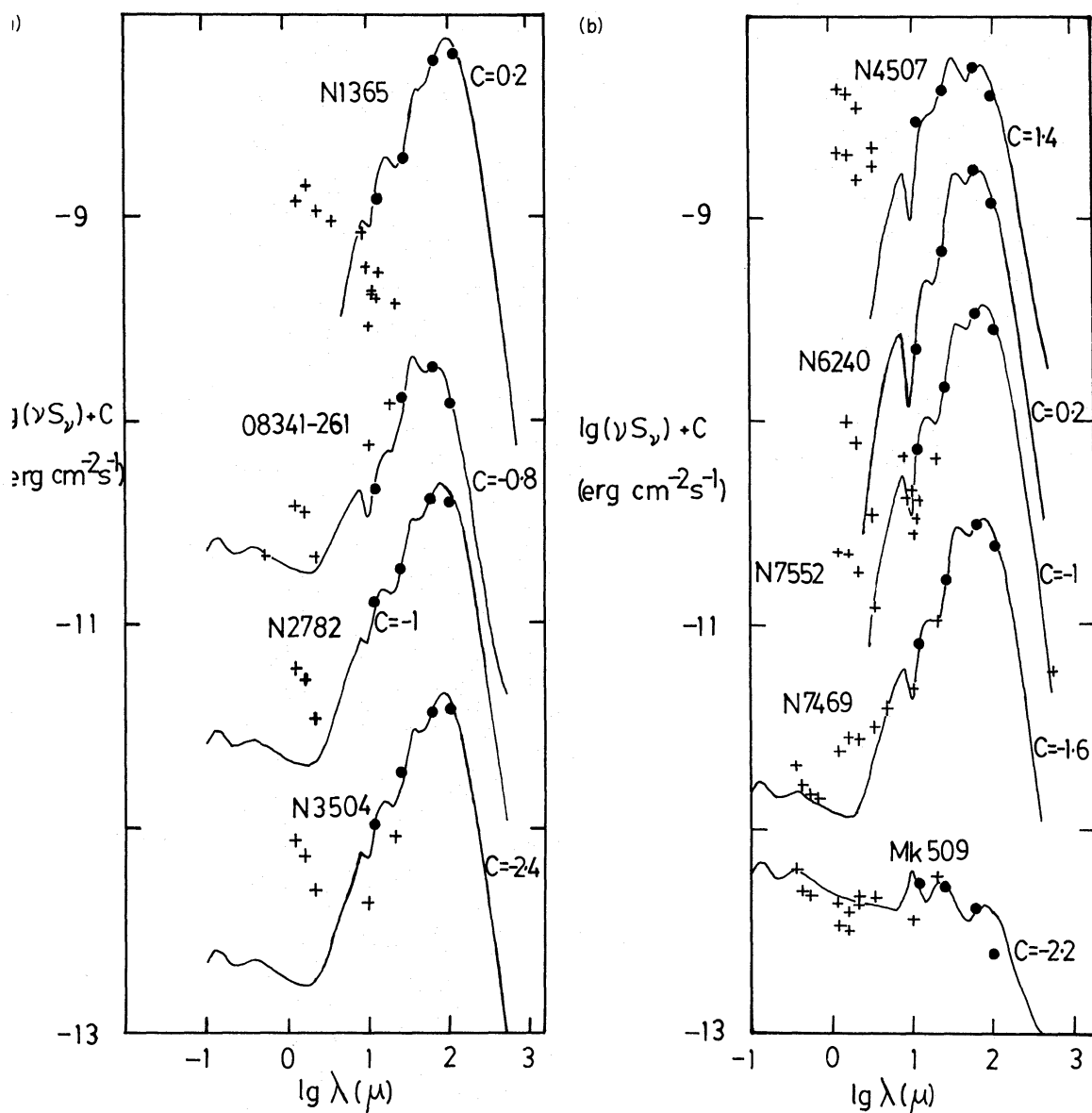
### 7.1 GALAXIES FOR WHICH THE MODELS OF SECTION 4 ARE A GOOD FIT

Fig. 9(a) and (b) shows the visible to far-infrared spectra of several galaxies for which the basic model of Section 4 gives a good fit. These include the galaxy NGC 6240, for which we attribute most of the far-infrared emission to a starburst component ( $\alpha_2 = 0.95$ ). The contribution of starlight can be seen at wavelengths shorter than 3  $\mu\text{m}$  (except for NGC 7469, for which it has been subtracted. Ward *et al.* 1987). Fig. 9(c) shows the data for 3C273 compared with our three-component model and for the model of Section 5 with an additional pure power-law component. Although the latter improves the fit to the *IRAS* data, the fit to the overall spectrum is not improved. The most obvious deficiency of our three-component model for 3C 273 is the failure to account for the 2–4  $\mu\text{m}$  ‘bump’ noted by Edelson & Malkan (1986). Models for this feature will be presented subsequently.

### 7.2 GALAXIES FOR WHICH A HIGHER-OPTICAL-DEPTH ‘SEYFERT’ COMPONENT IS REQUIRED

The best observed galaxy in this category is NGC 1068. Fig. 9(d) shows the spectrum of the core ( $\leq 100$  pc) of this galaxy compared with a high-optical-depth model ( $\beta = 1$ ,  $T_1 = 500$  K,  $\tau_{\text{uv}} = 75$ ,  $r_1/r_2 = 0.00215$ ). The latter model, which involves a dust mass of  $3 \times 10^5 M_{\odot}$  distributed between 4 and 180 pc from the central power-law source, is a much better fit to the observations than our standard ‘Seyfert’ component.

On rerunning our deconvolution programme with this higher-optical-depth ‘Seyfert’ model, there are several other galaxies for which this gives a much better fit to the overall spectra,



**Figure 9.** Ultraviolet to millimetre wavelength spectra predicted by the models of the present paper, compared with observations, for selected galaxies. The filled circles are the colour-corrected *IRAS* data, to which the models were fitted, and crosses are data from literature cited.

(a) NGC 1365, 08341-261, NGC 2782, NGC 3504. References for observations: Phillips & Frogel (1980), Frogel, Elias & Phillips (1982), Allen, Wright & Goss (1976), Balzano & Weedman (1981), Lebofsky & Rieke (1979).

(b) NGC 4507, 6240, 7552, 7469 and Mkn 509. References for observations: Ward *et al.* (1982), Glass (1981), Allen (1976), Frogel *et al.* (1982), Hildebrand *et al.* (1977), Lawrence *et al.* (1985), Balzano & Weedman (1981).

namely NGC 1275, 1386, 3783, 5253 and 6764 and Mkn 3 and 231, illustrated in Fig. 9(c) and (e).

A few other galaxies appear to require an intermediate-optical-depth Seyfert component. Fig. 9(f) shows fits of I Zw 1, Mkn 79, NGC 3516 and IC 4329A to a model with  $\beta = 1$ ,  $T_1 = 1000$  K,  $\tau_{uv} = 20$ ,  $r_1/r_2 = 0.0052$ . Parameters for these models are given in Table 4. Starlight has been subtracted for Mkn 79 (Ward *et al.* 1987). Many of these Seyferts, whose infrared spectra correspond to high-optical-depth dust clouds, have power-law continua in the

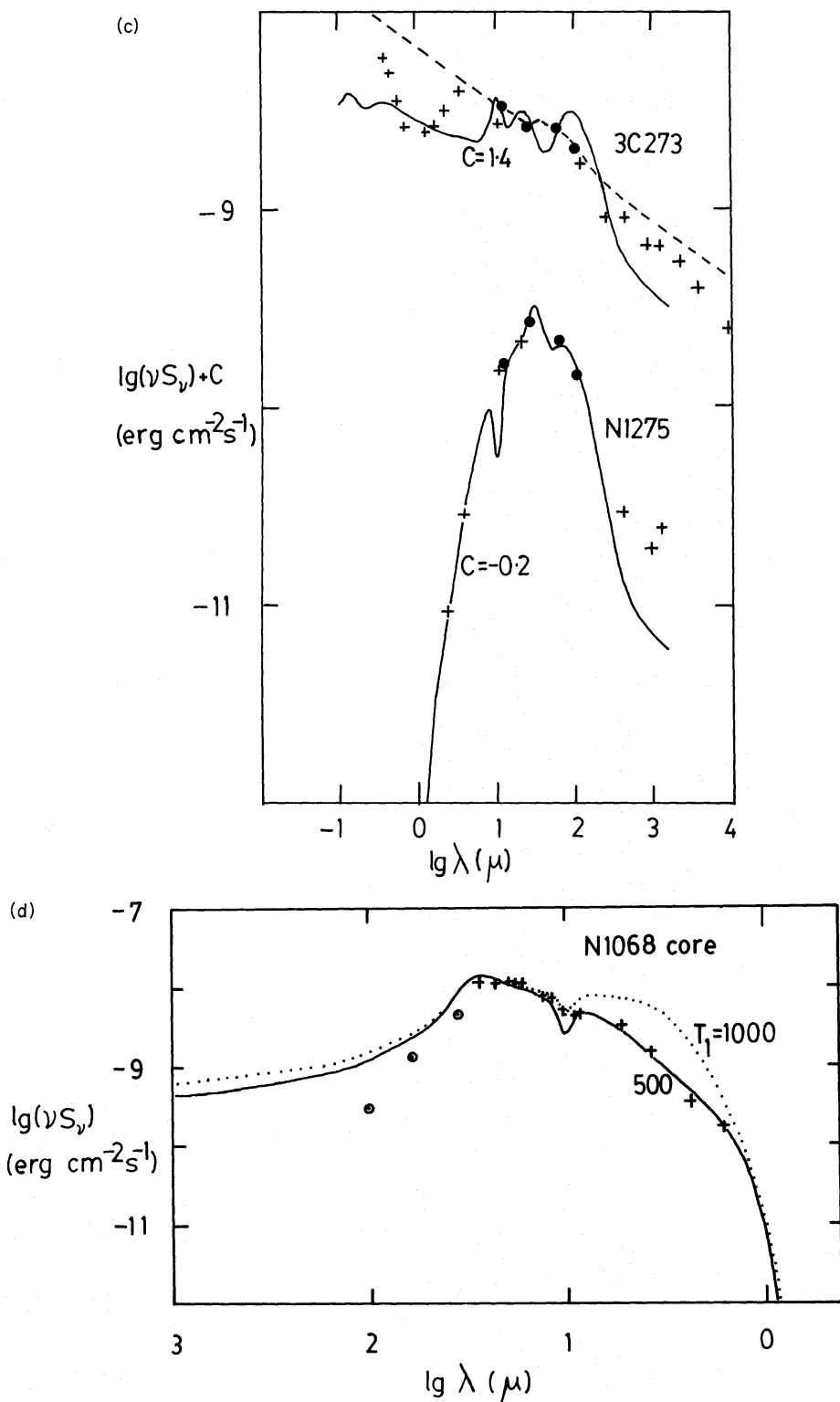
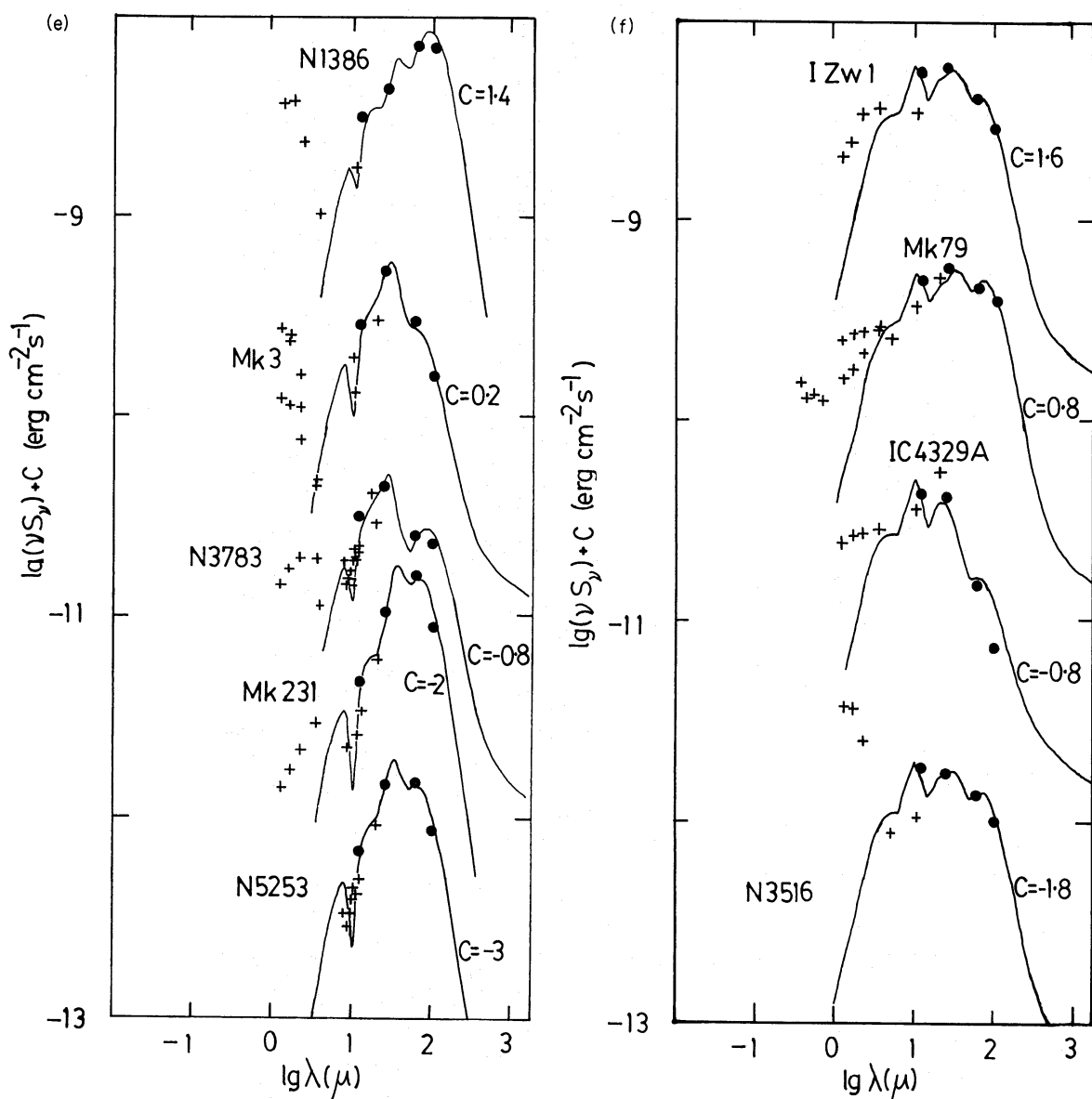


Figure 9 – continued

(c) 3C 273 (solid curve: three-component model, broken curve: four-component model – in fact only the ‘quasar’ and ‘starburst’ components are present). NGC 1275 ( $\tau_{uv} = 75$ ,  $T_i = 500$  K model, see Fig. 9d). References for observations: Neugebauer *et al.* (1976), Clegg *et al.* (1983), Gear *et al.* (1984), the latter two sets contemporaneous with the IRAS observations.

(d) The core of NGC 1068 (data from Telesco *et al.* 1984) compared with  $\tau_{uv} = 75$  Seyfert model, with  $T_i = 1000$  K (dotted curve) and 500 K (solid curve).

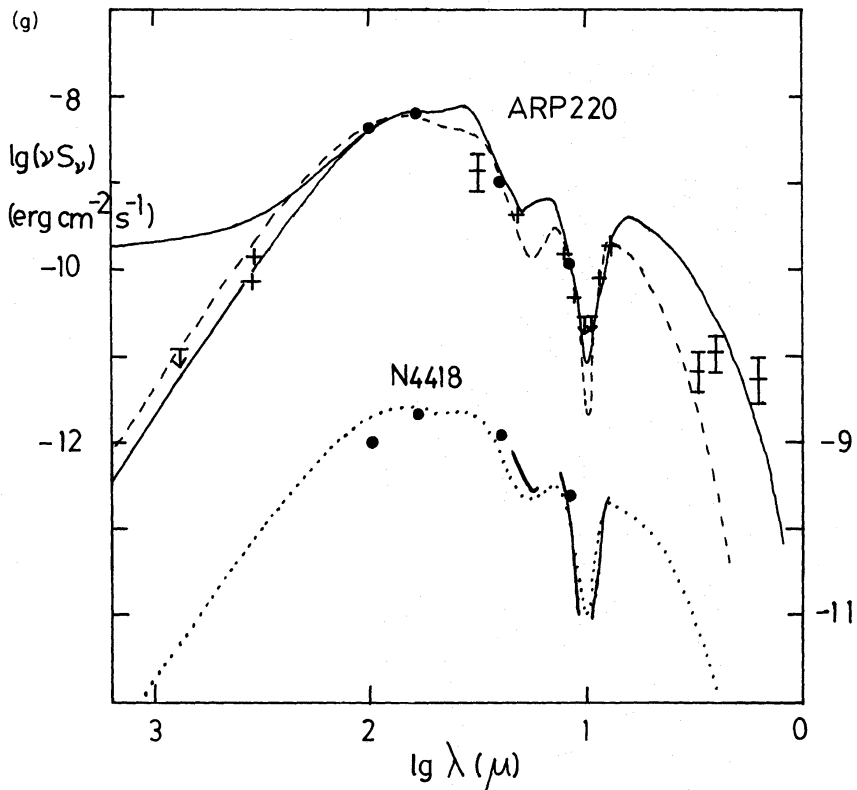


**Figure 9 – continued**

(e) Galaxies for which the  $\tau_{uv} = 75$ ,  $T_i = 500$  K model of Fig. 3(d) gives a better fit to the overall spectrum than our standard model: NGC 1386, Mkn 3, NGC 3783, Mkn 231, NGC 5253. References for observations: Phillips & Frogel (1980), Rieke (1978), Neugebauer *et al.* (1976), Frogel *et al.* (1982), Glass, Moorwood & Eichenhoof (1982), Allen (1976), McAlary, McLaren & Crabtree (1979).

(f) Galaxies for which a  $\tau_{uv} = 20$ ,  $T_i = 1000$  K model (Fig. 3d) gives a better fit to the overall spectrum than our standard model: I Zw 1, Mkn 79, IC 4329A, NGC 3516. References for observations: Rieke (1978), Ward *et al.* (1987), McAlary *et al.* (1979).

ultraviolet showing little indication of extinction by dust. There is therefore a contradiction between the value of  $\tau_{uv}$  inferred along the line-of-sight to the Seyfert nucleus ( $< 1$ ) and that inferred from the emission spectrum of the dust at infrared wavelengths ( $\gg 1$ ). The natural inference is that the dust in the Seyfert narrow-line region is concentrated into high-optical-depth clouds, which allow some fraction of the optical to X-ray luminosity to escape, directly or indirectly, along the line-of-sight. Seyferts which show both re-emission from high-optical-depth clouds, and have strong optical to X-ray emission, will be those with no cloud along the

**Figure 9 – continued**

(g) Models for Arp 220 (broken curve: ‘starburst’ model with an additional  $A_v = 78$  mag of extinction by interstellar dust. Solid curve: power-law ( $\alpha = 0.7$ ) continuum source embedded in uniform spherically symmetric dust cloud with  $\tau_{uv} = 186$  ( $A_v = 40$ ). The upper and lower solid curves at larger wavelengths correspond to whether the power-law source continues beyond  $100 \mu\text{m}$  or not) and NGC 4418 (RH scale, dotted curve: ‘starburst’ model with an additional  $A_v = 39$  mag of extinction by interstellar dust). References for observations: Emerson *et al.* (1984), Becklin & Wynn-Williams (1987), Roche *et al.* (1986).

line-of-sight. Type 2 Seyferts may simply be cases in which there is a cloud along the line-of-sight (*cf.* the review by Lawrence 1987).

### 7.3 Arp 220

Fig. 9(g) shows two possible models for the unusual galaxy Arp 220. This galaxy does not actually qualify for the sample studied in the present paper, since the  $12-\mu\text{m}$  flux value is not of sufficient quality, but the interest generated by it (Soifer *et al.* 1985; Becklin & Wynn-Williams 1987) warrants trying to understand its far-infrared spectrum within the framework of the present paper.

The *IRAS* colours of this galaxy are unique (for example,  $\log[S(25)/S(12)] = 1.25$ ) and it cannot be understood as a mixture of the three components used in Section 4. It can, however, be modelled either as a starburst behind very strong ( $A_v = 78$  mag) interstellar extinction (arising perhaps because the galaxy is seen virtually edge-on), or as a quasar embedded in a high-optical-depth ( $\tau_{uv} = 186$ ,  $A_v = 40$ ) dust cloud. The predicted outer angular radii of the dust clouds are 1.3 arcsec for the starburst model with extinction and 0.37 arcsec for the embedded quasar model, and, since the  $20-\mu\text{m}$  emission tends to come from the inner edge of the dust cloud, these are both consistent with the  $\leq 1$  arcsec size at  $20 \mu\text{m}$  reported by Becklin & Wynn-Williams (1987).

**Table 5.** Parameters for additional models discussed in Section 7.(a)  $\tau_{uv} = 75$ ,  $T_1 = 500$  K ‘Seyfert’ component.

Identification	$\alpha_1$	$\alpha_2$	$\alpha_3$	$\sigma$	$\log L_D$	$\log L_B$	$\log L_S$
N 1068	0.254	0.193	0.553	0.076	10.94	10.82	11.28
N 1275	0.082	0.415	0.503	0.004	10.35	11.05	11.14
N 1386	0.350	0.462	0.188	0.012	9.67	9.80	9.41
Mk 3	—	0.343	0.664	0.017	—	10.57	10.85
N 3783	0.212	0.110	0.678	0.012	9.98	9.70	10.49
Mk 231	—	0.881	0.129	0.010	—	12.63	11.80
N 5253	—	0.675	0.333	0.017	—	9.16	8.85

(b)  $\tau_{uv} = 20$  ‘Seyfert’ component.

I Zw 1	—	0.455	0.537	0.023	—	11.75	11.83
Mk 79	0.070	0.460	0.457	0.041	9.85	10.57	10.66
I 4329A	—	0.226	0.779	0.041	—	10.41	10.95
N 3516	0.045	0.415	0.539	0.006	—	9.93	10.04

(c) Four-component model (+ ‘quasar’).

Identification	$\alpha_1$	$\alpha_2$	$\alpha_3$	$\alpha_4$	$\sigma$	$L_D$	$L_B$	$L_S$	$L_Q$
N 3516	—	0.138	0.225	0.637	0.015	—	9.45	9.67	10.12
3C273	0.001	0.118	—	0.886	0.009	—	12.02	—	12.90
Mk 509	—	0.172	0.325	0.511	0.015	—	10.64	10.91	11.11

## 7.4 NGC 4418

This galaxy has an unusually high S(25)/S(12) ratio and a very deep 10- $\mu\text{m}$  absorption feature (Roche *et al.* 1986), both of which suggest exceptionally high extinction. It is located at  $l=290^\circ$ ,  $b=61^\circ$ , where the interstellar extinction is low. Our model for this (Fig. 9g) consists of a pure starburst with an additional  $A_v = 37$  mag of extinction, most of which is presumably due to internal extinction in NGC 4418, which would again have to be almost edge-on.

## 8 Discussion

The model fits to the far-infrared spectra of the assumed components, illustrated in Fig. 3, can be used to estimate the dimensions and masses of the dust clouds responsible for the infrared emission. For the ‘starburst’ and ‘Seyfert’ component models, which involve a specific optical depth in dust, the angular and linear radius of the dust cloud can be derived from the integrated flux,  $S_{\text{tot}}$  (equation 1) and the luminosity  $L_j$  (equation 7), respectively.

For the ‘starburst’ model we find, for a spherically symmetric cloud illuminated by a central cluster of stars,

$$\log(\theta_2/\text{arcsec}) = -6.81 + 0.5 \log(1.26 \alpha_2 S_{\text{tot}}) \quad (9)$$

and

$$\log(r_2/\text{cm}) = 15.6 + 0.5 \log(L_B/L_\odot).$$

The inner edge of the dust cloud is defined by

$$r_1/r_2 = 0.0015.$$

The corresponding dust mass is

$$\log(M_d/M_\odot) = -4.25 + \log(L_B/L_\odot). \quad (10)$$

For the galaxies in the present sample,  $r_2$  lies in the range 30–2500 pc, so the starburst activity is confined to a small region of the galaxy, presumably in most cases the nucleus. However, our assumption of spherical symmetry clearly underestimates the extent if the stars are distributed through the cloud or if the starburst is located in a ring. For example, for the NGC 1068 ‘starburst’ component we find  $\theta_2 = 3$  arcsec and  $r_2 = 350$  pc, considerably smaller than the observed 3-kpc diameter ring.

If the starburst consists of  $n$  similar non-overlapping clouds, then  $\theta_2$  and  $r_2$  in equation (9) should be reduced by  $n^{1/2}$ : they then refer to the size of an individual cloud. Equation (10) is unaltered. If each cloud is a typical giant molecular cloud of  $10^5 M_\odot$ , containing  $\sim 10^3 M_\odot$  in dust, then  $n \sim 1$  for  $L_B = 10^7 L_\odot$  and  $n \sim 10^5$  for  $L_B = 10^{12} L_\odot$ .

For the ‘Seyfert’ model we find, for a spherically symmetric geometry,

$$\log(\theta_2/\text{arcsec}) = -7.32 + 0.5 \log(1.26 \alpha_3 S_{\text{tot}}) \quad (11)$$

and

$$\log(r_2/\text{cm}) = 15.11 + 0.5 \log(L_S/L_\odot),$$

with a corresponding dust mass

$$\log(M_D/M_\odot) = -7.81 + \log(L_S/L_\odot). \quad (12)$$

The inner edge of the dust cloud is defined by

$$r_1/r_2 = 0.0055.$$

For the galaxies in the present sample,  $r_2$  lies in the range 30–400 pc, consistent with the dust being located in the narrow-line region of the Seyfert nucleus.

The gas in Seyfert narrow-line regions is known to be highly clumpy, with a very low filling-factor. Evidence that the same is true for the dust was given in Section 7. The parameters of our model deduced using equations (11) and (12) would still be broadly correct, provided there are several clumps along an average line-of-sight to the illuminating source. If this is the case, the actual radius of the region,  $R$ , will be related to our inferred size  $r_2$  by

$$R \sim C^{-1/2} r_2,$$

where  $C$  is the covering factor.

The small linear extents deduced for our ‘starburst’ and ‘Seyfert’ components are consistent with the observed compactness of the 10- $\mu\text{m}$  sources in IRAS galaxies with  $S(25)/S(60) > 0.3$  (Hill 1987) and with Seyfert or H II region nuclei (Devereux 1987).

For the ‘disc’ model we assumed  $\tau_\nu \propto \nu$ , but the model does not involve any specific value of  $\tau_{uv}$  so we can only calculate  $\tau_{100}^{1/2} \theta_2$ , where  $\tau_\nu = \tau_{100}$  (100  $\mu\text{m}/\lambda$ ) is the optical depth in 30-K grains. We find

$$\log[\tau_{100}^{1/2}(r_2/\text{cm})] = 16.02 + 0.5 \log(L_D/L_\odot), \quad (13)$$

or

$$\log[\tau_{100}^{1/2}(\theta_2/\text{arcsec})] = -6.90 + 0.5 \log(1.26 \alpha_1 S_{\text{tot}}).$$

The optical depth at 12  $\mu\text{m}$  in 210-K grains,  $\tau_{12}$ , is related to that in 30-K grains by  $\tau_{12} = 0.98 \times 10^{-4} \tau_{100}$ . For a source to be a point source at 60 and 100  $\mu\text{m}$ , the full width to half-power cannot be greater than 1 arcmin. Galaxies with  $\alpha_1 > 0.5$  yield  $\tau_{100}^{1/2}(\theta_2/\text{arcsec})$  in the

range 0.6–1.2 arcsec and this implies  $\tau_{100} \geq 0.0004$ . Using the interstellar grain model of Rowan-Robinson (1986), we can translate this lower limit on  $\tau_{100}$  to one on  $A_v$  (assuming  $\tau_{100}$  refers only to the warmer,  $a \leq 0.03\text{-}\mu\text{m}$  radius grains) and find  $A_v \geq 0.8$ . This is broadly consistent with the optical-depth estimates derived from Fig. 4. Since many of the galaxies in the present sample have Holmberg diameters considerably greater than 1 arcmin, we must presume that the bulk of the far-infrared emission comes from the inner part of the galaxy. This is still consistent with it being re-emission of starlight obscured by interstellar dust, since the expected half-power width is much smaller than the Holmberg diameter.

## 9 Conclusions and further work

- (i) The 12–100  $\mu\text{m}$  *IRAS* spectra of galaxies are naturally understood in terms of three components: a cool ‘disc’ component, a warm ‘starburst’ component, and a hot ‘Seyfert’ component.
- (ii) The ‘disc’ component can be modelled as emission by interstellar dust of energy absorbed from the general stellar radiation field, the ‘cirrus’ in our own Galaxy. Incorporation of a detailed model for very small grains is a priority for further theoretical work.
- (iii) The ‘starburst’ component can be modelled in terms of an optically thick dust cloud illuminated by newly formed massive stars. A third of galaxies with  $L_B/L_{\text{opt}} > 4$  have values of  $L_D/L_{\text{opt}}$  too high to be consistent with the simple ‘cirrus’ model and deserve further study. They may be cases where the internal extinction is exceptionally high, though this is not reflected in anomalously high values of S(25)/S(12).
- (iv) The ‘Seyfert’ component can be modelled as emission from dust in the narrow-line region, with an  $r^{-1}$  density distribution, absorbing the Seyfert’s power-law continuum. There is evidence that the dust is concentrated into clouds. Further observations are needed to understand why Seyferts have such low values of  $L_D/L_{\text{opt}}$ .

## References

- Allen, D. A., 1976. *Astrophys. J.*, **207**, 367.  
 Allen, D. A., Wright, A. E. & Goss, W. M., 1976. *Mon. Not. R. astr. Soc.*, **177**, 91.  
 Balzano, V. A., 1983. *Astrophys. J.*, **268**, 602.  
 Balzano, V. A. & Weedman, D. W., 1981. *Astrophys. J.*, **243**, 756.  
 Becklin, E. E. & Wynn-Williams, C. G., 1987. In: *Star Formation in Galaxies*, p. 643, ed. Persson, C., NASA CP-2466.  
 Boulanger, F., Baud, B. & van Albada, G. D., 1985. *Astr. Astrophys.*, **144**, L9.  
 Branduardi-Raymond, G., Fabricant, D., Feigelson, E., Gorenstein, P., Grindlay, J., Soltan, A. & Zamorani, G., 1981. *Astrophys. J.*, **248**, 55.  
 Burstein, D. & Heiles, C., 1978. *Astrophys. J.*, **225**, 40.  
 Burton, W. B., Deul, E. R., Walker, H. J. & Jongeneelen, A. A. W., 1986. In: *Light on Dark Matter, Proc. 1st IRAS Conf.*, p. 357, ed. Israel, F. P., Reidel, Dordrecht.  
 Carleton, N. P., Elvis, M., Fabbiano, G., Lawrence, A., Ward, M. J. & Willner, S. P., 1987. *Astrophys. J.*, **318**, 295.  
 Carter, D., 1984. *Astronomy Express*, **1**, 61.  
 Caux, E. & Serra, G., 1986. *Astr. Astrophys.*, **165**, L5.  
 Cheney, J. & Rowan-Robinson, M., 1981. *Mon. Not. R. astr. Soc.*, **195**, 831.  
 Clegg, P. E., Gear, W. K., Ade, P. A. R., Robson, E. I., Smith, M. G., Nolt, I. G., Radostitz, J. V., Glaccum, W., Harper, D. A. & Low, F. J., 1983. *Astrophys. J.*, **273**, 58.  
 Cox, P. & Mezger, P. G., 1988. In: *Comets to Cosmology*, ed. Lawrence, A., Springer-Verlag, Berlin.  
 Crawford, J. & Rowan-Robinson, M., 1986. *Mon. Not. R. astr. Soc.*, **221**, 923.  
 da Costa, C. N., Nunes, M. A., Pellegrini, P. S., Willner, C., Chincarini, G. & Cowan, J. J., 1985. *Astr. J.*, **91**, 6.  
 de Grijp, M. H. K., Miley, G. k., Lub, J. & de Jong, T., 1985. *Nature*, **314**, 240.  
 de Jong, T. & Brink, K., 1987. In: *Star Formation in Galaxies*, p. 323, ed. Persson, C., NASA CP-2466.

- DePoy, D. L., Becklin, E. E. & Wynn-Williams, C. G., 1986. *Astrophys. J.*, **116**, 96.
- de Vaucouleurs, G., de Vaucouleurs, A. & Corwin, H., Jr, 1976. *2nd Reference Catalogue of Bright Galaxies*, University of Texas, Austin.
- Devereux, N., 1987. In: *Star Formation in Galaxies*, ed. Persson, C., NASA CP-2466.
- Draine, B. T. & Anderson, N., 1985. *Astrophys. J.*, **292**, 494.
- Edelson, R. A. & Malkan, M. A., 1986. *Astrophys. J.*, **308**, 59.
- Edelson, R. A., Malkan, M. A. & Rieke, G. H., 1987. *Astrophys. J.*, **321**, 233.
- Elvis, M. & Lawrence, A., 1989. *Astrophys. J.*, in press.
- Emerson, J., Clegg, P. E., Gee, G., Cunningham, C. T., Griffin, M. J., Brown, L. M. C., Robson, E. I. & Longmore, A. J., 1984. *Nature*, **311**, 237.
- Frogel, J. F., Elias, J. H. & Phillips, M. M., 1982. *Astrophys. J.*, **260**, 70.
- Gautier, T. N. & Beichman, C. A., 1985. *Bull. Am. Astr. Soc.*, **16**, 968.
- Gear, W. K., Robson, E. I., Ade, P. A. R., Smith, M. G., Clegg, P. E., Cunningham, C. T., Griffin, M. J., Nolt, I. G. & Radostitz, J. V., 1984. *Astrophys. J.*, **280**, 102.
- Glass, I. S., 1981. *Mon. Not. R. astr. Soc.*, **197**, 1067.
- Glass, I. S., Moorwood, A. F. M. & Eichenhoof, W., 1982. *Astr. Astrophys.*, **107**, 276.
- Habing, H. J., Olnon, F. M., Chester, T., Gillett, F., Rowan-Robinson, M. & Neugebauer, G., 1985. *Astr. Astrophys.*, **152**, L1.
- Hawarden, T., 1986. In: *Light on Dark Matter*, ed. Israel, F. P., Reidel, Dordrecht.
- Hauser, M. G., Silverberg, R. F., Steir, M. T., Kelsall, T., Gezari, D. Y., Dwelz, E., Walser, D. & Mather, J. C., 1984. *Astrophys. J.*, **285**, 74.
- Helou, G., 1986. *Astrophys. J.*, **311**, L33.
- Hewitt, A. & Burbidge, G. R., 1980. *Astrophys. J. Suppl.*, **43**, 59.
- Hildebrand, R. H., Whitcomb, S. E., Winston, R., Stening, R. F., Harper, D. A. & Moseley, S. H., 1977. *Astrophys. J.*, **216**, 698.
- Hill, G. J., 1987. In: *Star Formation in Galaxies*, ed. Persson, C., NASA CP-2466.
- Huchra, J., 1988. *Redshift Catalog*, Harvard Smithsonian Center for Astrophysics.
- IRAS Explanatory Supplement*, 1984. Eds. Beichman, C. A., Neugebauer, G., Habing, H. J., Clegg, P. E. & Chester, T. J., JPLD-1855.
- Joseph, R. D. & Wright, G. S., 1985. *Mon. Not. R. astr. Soc.*, **214**, 87.
- Kriss, G. A., Canizares, C. R. & Ricker, G. R., 1980. *Astrophys. J.*, **242**, 492.
- Kron, G. E. & Shane, C. D., 1976. *Astrophys. Space Sci.*, **39**, 401.
- Lauberts, A., 1982. *The ESO-Uppsala Survey of the ESO(B) Atlas*, European Southern Observatory.
- Lawrence, A., 1987. *Publs astr. Soc. Pacif.*, **99**, 309.
- Lawrence, A. & Elvis, M., 1982. *Astrophys. J.*, **256**, 410.
- Lawrence, A., Ward, M., Elvis, M., Fabbiano, G., Willner, S. P., Carleton, N. P. & Langmore, A., 1985. *Astrophys. J.*, **291**, 117.
- Lebofsky, M. J. & Rieke, G. H., 1979. *Astrophys. J.*, **229**, 111.
- Leger, A. & Puget, J. L., 1984. *Astr. Astrophys.*, **137**, L5.
- Lonsdale, C. J., Helou, G., Good, J. C. & Rice, W., 1984. *Catalogued Galaxies and Quasars in the IRAS Survey*, JPLD-1932.
- Low, F. J. et al., 1984. *Astrophys. J.*, **278**, L19.
- McAlary, C. W., McLaren, R. A. & Crabtree, D. R., 1979. *Astrophys. J.*, **234**, 471.
- McHardy, I. M., Lawrence, A., Pye, J. P. & Pounds, K. A., 1981. *Mon. Not. R. astr. Soc.*, **197**, 893.
- Marshall, F. E., Boldt, E. A., Holt, S. S., Mushotzky, R. F., Pravdo, S. H., Rothschild, R. E. & Serlemitsos, P. J., 1979. *Astrophys. J. Suppl.*, **40**, 657.
- Mathis, J. S., Mezger, P. G. & Panagia, N., 1983. *Astr. Astrophys.*, **128**, 212.
- Miley, G. K., Neugebauer, G., Clegg, P. E., Harris, S., Rowan-Robinson, M., Soifer, B. T. & Young, E., 1984. *Astrophys. J.*, **278**, L79.
- Moorwood, A. F. M., Véron-Cetty, M.P. & Glass, I. S., 1986. *Astr. Astrophys.*, **160**, 39.
- Neugebauer, G., Becklin, E. E., Oke, J. B. & Searle, L., 1976. *Astrophys. J.*, **205**, 29.
- Neugebauer, G., Soifer, B. T. & Rowan-Robinson, M., 1986. In: *Structure and Evolution of Active Galaxy Nuclei*, p. 11, ed. Giurcin, G. et al., Reidel, Dordrecht.
- Neugebauer, G., Oke, J. B., Becklin, E. E. & Matthews, K., 1979. *Astrophys. J.*, **230**, 79.
- Nilson, P., 1973. *Uppsala General Catalogue of Galaxies*, Uppsala.
- Osterbrock, D. E. & de Robertis, M. M., 1985. *Publs astr. Soc. Pacif.*, **97**, 1129.
- Pajot, F., Gispert, P., Lamarre, J.-M., Peytureux, R., Pomerantz, M. A., Puget, J.-L. & Serra, G., 1986. *Space-Borne Sub-Millimetre Astronomy*, Mission-ESA Workshop, Segovia.
- Phillips, M. M. & Frogel, J. A., 1980. *Astrophys. J.*, **235**, 761.

- Richstone, D. O. & Schmidt, M., 1980. *Astrophys. J.*, **235**, 361.  
 Rieke, G. H., 1978. *Astrophys. J.*, **226**, 550.  
 Rieke, G. H., Cutri, R. M., Black, J. H., Kailey, W. F., McAlary, C. W., Labofsky, M. J. & Elston, R., 1985. *Astrophys. J.*, **290**, 116.  
 Roche, P. F., Aitken, D. K., Smith, C. H. & James, S. D., 1986. *Mon. Not. R. astr. Soc.*, **218**, 19P.  
 Rodrigues-Espinosa, J. A., 1987. In: *Star Formation in Galaxies*, p. 669, ed. Persson, C., NASA CP-2466.  
 Rowan-Robinson, M., 1977. *Astrophys. J.*, **213**, 635.  
 Rowan-Robinson, M., 1979. *Astrophys. J.*, **234**, 111.  
 Rowan-Robinson, M., 1980. *Astrophys. J. Suppl.*, **44**, 403.  
 Rowan-Robinson, M., 1982. *Mon. Not. R. astr. Soc.*, **201**, 289.  
 Rowan-Robinson, M., 1986. *Mon. Not. R. astr. Soc.*, **219**, 737.  
 Rowan-Robinson, M., 1987a. In: *Star Formation in Galaxies*, p. 133, ed. Persson, C., NASA CP-2466.  
 Rowan-Robinson, M., 1987b. In: *Starbursts and Galaxy Evolution*, p. 235, ed. Thuan, T. X., Montmerle, T. & Thanh van, J. T., Edition Frontières.  
 Rowan-Robinson, M. & Chester, T., 1987. *Astrophys. J.*, **313**, 413.  
 Rowan-Robinson, M. & Crawford, J., 1986. In: *Light on Dark Matter*, p. 421, ed. Israel, F., Reidel, Dordrecht.  
 Rowan-Robinson, M., Helou, G. & Walker, D., 1987. *Mon. Not. R. astr. Soc.*, **227**, 589.  
 Sandage, A. & Tammann, G. A., 1981. *Revised Shapley-Ames Catalog of Bright Galaxies*, Carnegie Institute, Washington.  
 Sellgren, K., 1984. *Astrophys. J.*, **277**, 623.  
 Soifer, B. T. et al., 1985. *Astrophys. J.*, **278**, L71.  
 Soifer, B. T., Sanders, D. B., Madore, B. F., Neugebauer, G., Danielson, G. E., Persson, C. J. & Rice, W. L., 1987. *Astrophys. J.*, **320**, 238.  
 Telesco, C. M., Becklin, E. E. & Wynn-Williams, G. G., 1984. *Astrophys. J.*, **282**, 427.  
 Véron-Cetty, M.-P. & Véron, P., 1985. *Catalogue of Quasars and Active Nuclei*, ESO, Munich.  
 Vorontsov-Velyaminov, B. A. et al., 1962–74. *Morphological Catalogue of Galaxies I–V*, Sternberg Institute, Moscow.  
 Ward, M., Allen, D. A., Wilson, A. S., Smith, M. G. & Wright, A. E., 1982. *Mon. Not. R. astr. Soc.*, **199**, 953.  
 Ward, M., Elvis, M., Fabbiano, G., Carleton, N., Willner, S. P. & Lawrence, A., 1987. *Astrophys. J.*, **315**, 74.  
 Weedman, D. W., 1973. *Astrophys. J.*, **183**, 29.  
 Wilson, A. S., 1987. In: *Star Formation in Galaxies*, p. 675, ed. Persson, C., NASA CP-2466.  
 Zwicky, F. et al., 1968. *Catalogue of Galaxies and Clusters of Galaxies*, California Institute of Technology.

### Appendix A: colour-correction of IRAS data

Colour corrections for the model components have been derived as follows (Table A1): at 12 and 100  $\mu\text{m}$  they are derived from power-law fits to the 25/12 and 100/60 flux ratios (using Table VI.C.6 of the *IRAS* Introductory Supplement 1984). For 25  $\mu\text{m}$  the corrections are the averages of the values derived from the 25/12 and 60/25 flux ratios and for 60  $\mu\text{m}$  they are the average of the values derived from the 60/25 and 100/60 flux ratios.

**Table A1.** Adopted  $K_{j,i}$

	$\lambda =$	12	25	60	100 $\mu\text{m}$
	$i =$	1	2	3	4
$D, \quad j=1$		1.10	1.00	1.00	1.005
$B, \quad j=2$		0.93	0.93	1.02	1.01
$S, \quad j=3$		0.985	1.05	1.09	1.03
( $\tau_{uv} = 75$ model)		0.96	0.99	1.08	1.04
( $\tau_{uv} = 20$ model)		1.22	1.10	1.04	1.02
$Q, \quad j=4$		1.02	1.02	1.01	1.00

After solution for the  $\alpha_j$  (Section 5), the *IRAS* fluxes plotted in Fig. 9 are corrected using

$$S_i(\text{corr}) = S_i(\text{IRAS}) / K_i,$$

where

$$1/K_i = \sum_j \alpha_j t_{j,i} K_{j,i} / \sum_j \alpha_j t_{j,i}$$

and  $t_{j,i}$  is defined in Section 5 (equation 4).